

SANDIA REPORT

SAND86—1866 • UC—62

Unlimited Release

Printed February 1987

RS-8232-2/65390

C. I

CIRCE.001: A Computer Code for Analysis of Point-Focus Concentrators with Flat Targets



8232-2/065390



00000001 -

A. C. Ratzel, B. D. Boughton

Prepared by
Sandia National Laboratories
Albuquerque, New Mexico 87185 and Livermore, California 94550
for the United States Department of Energy
under Contract DE-AC04-76DP00789

1054223

Issued by Sandia National Laboratories, operated for the United States Department of Energy by Sandia Corporation.

NOTICE: This report was prepared as an account of work sponsored by an agency of the United States Government. Neither the United States Government nor any agency thereof, nor any of their employees, nor any of their contractors, subcontractors, or their employees, makes any warranty, express or implied, or assumes any legal liability or responsibility for the accuracy, completeness, or usefulness of any information, apparatus, product, or process disclosed, or represents that its use would not infringe privately owned rights. Reference herein to any specific commercial product, process, or service by trade name, trademark, manufacturer, or otherwise, does not necessarily constitute or imply its endorsement, recommendation, or favoring by the United States Government, any agency thereof or any of their contractors or subcontractors. The views and opinions expressed herein do not necessarily state or reflect those of the United States Government, any agency thereof or any of their contractors or subcontractors.

Printed in the United States of America
Available from
National Technical Information Service
U.S. Department of Commerce
5285 Port Royal Road
Springfield, VA 22161

NTIS price codes
Printed copy: A04
Microfiche copy: A01

SAND86-1866

**CIRCE.001: A Computer Code for Analysis of
Point-Focus Concentrators with Flat Targets¹**

February 11, 1987

A. C. Ratzel and B. D. Boughton
Fluid and Thermal Sciences Department 1510

Sandia National Laboratories
Albuquerque, NM 87185
Operated by
Sandia Corporation
for the U.S. Department of Energy

¹This work supported by the U. S. Department of Energy under contract number DE-AC04-76DP00789.

This page is intentionally left blank.

Abstract

In this report, a computer simulation code called **CIRCE** is discussed and examples of its application to several solar collector geometries are presented. **CIRCE**, an acronym for Convolution of Incident Radiation with Concentrator Errors, was developed for the optical analysis of point-focus concentrating dish collector systems. **CIRCE**, as in Greek mythology, is the “daughter” of **HELIOS**, a computer code developed at Sandia National Laboratories, Albuquerque, NM, for evaluating the optical performance of solar central receiver systems. **CIRCE** was developed from **HELIOS** specifically for the analysis of dish systems with the objective of providing users with a design tool that is relatively easy to implement and does not require a large investment of time to obtain results.

The solution techniques of **CIRCE**, in which the concentrator errors are convolved with the solar intensity profile (sunshape) to produce the flux density distribution on an arbitrary target, are identical to those used in **HELIOS**. **CIRCE** may be used to analyze reflectors that are spherical, parabolic, or flat and are either a continuous or faceted surface. Additionally, a polynomial fit for the facet contour is available for modeling concentrators such as the stretched membrane reflectors. The curvature and aim point of each optical facet that comprises the reflector may be individually assigned. The current version of **CIRCE**, referred to as **CIRCE.001**, is restricted to analyses of reflector systems with flat rectangular or circular targets. Future upgrades will allow two-dimensional axisymmetric external or internal cavity target geometries to be analyzed. Currently, user inputs include the concentrator geometry, the reflectivity, specularity, and slope error of the optical surface, the collector tracking error, the insolation level and sunshape. Output from the code includes a two-dimensional flux density map along the target surface, a “hit” map which indicates the number of facets contributing to the flux at a point on the target, and the concentrator optical efficiency.

CIRCE has been developed with the philosophy that “user-friendliness” is a necessity. Therefore, we have also developed an interactive data file generator **DEKGEN**, a graphics package **PLOT**, that utilizes **DISSPLA** software, and a procedural file that executes this suite of computer codes on a VAX system. In addition, procedures have been developed for executing **CIRCE** and **DEKGEN** on IBM-compatible personal computers. Important features of **CIRCE** and the subsidiary codes are provided in this report as are several examples of the use of **CIRCE** for optical performance calculations of both faceted and continuous reflector systems.

Contents

1	Introduction	1
2	Overview of CIRCE Numerical Modeling	3
2.1	Incident Flux on Target	5
2.2	Effective Sunshape	7
3	CIRCE Structure	11
4	Data File Generation	12
4.1	General Problem Parameters	14
4.2	Sun and Error Parameters	14
4.3	Target/Receiver Parameters	16
4.4	Reflector/Facet Parameters	18
5	CIRCE Output	22
6	Illustrative Examples	24
6.1	Example 1: Spherical and Parabolic Dishes	25
6.2	Example 2: One Vs. Three Facet Reflector Performances	28
6.3	Example 3: Test Bed Concentrator #1	31
7	CIRCE Usage	34
7.1	Implementation on VAX Computer Systems	34
7.2	Implementation on Personal Computer Systems	37
7.3	Execution Time Comparisons	38
8	Example Data Files and Output	40
9	References	41
A	Variables Used in DEKGEN	42
B	Example Data Files and Results	45
B.1	Example 1: 45° Rim Angle Parabolic Dish	45
B.1.1	45DEG.DAT File	45
B.1.2	Partial Results from 45DEG.OUT	46
B.2	Example 2: 3 Parabolic Facet Concentrator	48
B.2.1	3PDISH.DAT File	48
B.2.2	Partial Results from 3PDISH.OUT	49

List of Tables

1	Reflector Subfacets as a Function of Radial Subdivisions	19
2	Heat Flux Distributions – Polynomial Fits Compared with Spherical Curvature Results	21
3	Reflector and Tracking Error Budget	24
4	CIRCE Execution Times in Seconds for Example 2	39

List of Figures

1	Photograph of a LaJet LEC460 Concentrator located at SNLA.	4
2	Photograph of the General Electric 7-m parabolic dishes located at Shenandoah, Georgia.	4
3	Reflector–target geometry modeled by CIRCE	5
4	Typical sunshape distributions used in CIRCE and HELIOS	7
5	Geometry of target point P and the reflected–ray reference plane.	10
6	Schematic of a concentrator/target in the dish coordinate system used in the CIRCE simulation	13
7	Six limb options for pillbox sun	15
8	1–D effective sunshape used in examples.	25
9	Comparative results for 3 parabolic dishes ($f/d=0.43, 0.6, 0.93$).	26
10	Comparative results for 3 spherical dishes ($f/d=0.6, 0.8, 1.0$).	27
11	Projected view of single dish and 3 facet reflector systems modeled by CIRCE	29
12	Collector optical efficiency for single dish and 3 facet reflector systems	29
13	Schematic of canting effects on performance of parabolic dishes.	30
14	Incident flux profiles on targets from a single parabolic dish (a) and from the 3 parabolic facet reflector system (b).	30
15	Photograph of Test Bed Concentrator #1 at SNLA.	32
16	Center positions of 220 facets comprising TBC–1.	32
17	Incident heat flux (a) and collector optical efficiency (b) for the TBC–1 reflector system.	33
18	Execution sequence of CIRCE simulation on personal computer and VAX computer systems.	35
19	Recommended directory structure for executing CIRCE simulation.	36

Acknowledgement

The authors thank F. Biggs (7112), C. N. Vittitoe (2322), and G. P. Mulholland (New Mexico State University, Department of Mechanical Engineering) for their help during the development of the **CIRCE** simulation. Consultations with Frank Biggs and Charles Vittitoe were especially helpful during the debugging of **CIRCE**. George Mulholland was also an invaluable aid, providing us with test comparisons using **HELIOS**. Without the support of these three individuals, the **CIRCE** simulation development would have been made much more difficult.

Additionally, we thank B. Baker for developing software for executing **CIRCE** on IBM-compatible personal computers and for modifying the VAX computer version of **CIRCE** to execute on the PC. Finally, we acknowledge R. Diver and T. Mancini (6227), who have encouraged and helped to direct this work.

Nomenclature

Symbols

A_j	Reflector subfacet area	[m ²]
B_j	Target blockage factor	
d	Diameter of reflector dish	[m]
D_{ij}	Defined by Eq.(2)	[m ⁻²]
E	Error distribution	
E_s	Effective sunshape distribution	
f	Focal length of parabolic facet	[m]
F_{ij}	Flux incident on target point i from subfacet j	[W/m ²]
I	Solar intensity	[W/m ²]
L	Limb darkening distribution	
\hat{N}_i	Unit normal vector	
N_F	Number of subfacets per facet	
N_T	Total number of reflector subfacets	
r	Major axis extent for elliptic normal error distribution	[milliradians]
\bar{r}	Radial extent for circular normal error distribution	[milliradians]
r_{dish}	Parabolic dish radius	[m]
R	Radial position on circular facet	[m]
\mathcal{R}	Radius of curvature for spherical facets	[m]
s	Minor axis extent for elliptic normal error distribution	[milliradians]
S	Sunshape distribution	
\bar{S}	Normalized sunshape distribution	
S_l	Slant length from subfacet to target point	[m]
x	X-coordinate position	[m]
y	Y-coordinate position	[m]
z	Z-coordinate position	[m]
Z	Facet displacement (contour)	[m]

Nomenclature (contd.)

Greek

α	Angle (see Figure 3)	[degrees]
α	Start of sun limb	[milliradians]
β	Edge of sun limb	[milliradians]
η	Parabolic dish rim angle	[degrees]
η_{opt}	Concentrator optical efficiency	
θ	Rotation angle for elliptic normal error distribution	[degrees]
θ	Circumferential angle on circular target	[degrees]
μ	Incidence angle on reflector subfacet (see Figure 3)	[degrees]
ρ	Angle with respect to sun central ray	[milliradians]
ρ_s	Reflector solar specular reflectivity	
σ	Standard deviation of error	[milliradians]
ϕ	Incidence angle on target (see Figure 3)	[degrees]

Subscripts

<i>edge</i>	Edge of sunshape limb
<i>r</i>	Pertaining to major axis of elliptic normal error distribution
<i>s</i>	Pertaining to minor axis of elliptic normal error distribution
<i>slope</i>	Pertaining to slope error
<i>t, tot</i>	Pertaining to effective or total error
<i>target</i>	Pertaining to target
<i>1D</i>	One-dimensional
<i>2D</i>	Two-dimensional

Abbreviations

CIRCE	Convolution of Incident Radiation with Concentrator Errors
PC	Personal computer
SNLA	Sandia National Laboratories, Albuquerque, NM
STTF	Solar Thermal Test Facility of SNLA
TBC-1	Test Bed Concentrator #1
VDI	Virtual device interface
1-D	One-dimensional
2-D	Two-dimensional

Preface

The **CIRCE** simulation described in this report was developed from **HELIOS**, which was created by F. Biggs and C. N. Vittitoe during the 1970s principally for modeling central receiver solar energy collection systems. **HELIOS** was developed with flexibility in mind so that it could also be used for evaluating parabolic dish and trough solar collector systems. Indeed, much of the 2-m parabolic trough analysis work performed by A. C. Ratzel in the late 1970s used the **EDEP** optics subroutine package that was being developed concurrently with **HELIOS** by Biggs and Vittitoe.

More recently, efforts have been initiated to evaluate the optical and thermal performance capabilities of point-focus or dish solar collector systems. While, in theory, **HELIOS** could be used for these optics calculations, we determined that a dish-specific optics package utilizing the modeling theory of **HELIOS** would be superior to using **HELIOS** in its current format. To use **HELIOS**, update files would have to be constructed for the many different faceted and continuous-surface reflector systems to be considered, and this would require a working knowledge of the many coordinate systems in **HELIOS** and of the internal source code structure. Instead, we configured **CIRCE** from **HELIOS** to be a stand-alone code. Principally, we have simplified and streamlined the **HELIOS** simulation, and have restructured the algorithm to be more amenable to dish analyses. Presently, **CIRCE.001** will provide flux density profiles on flat targets; future generations of this simulation will be useful for providing flux profiles on 2-D axisymmetric external or internal receiver geometries, much needed for thermal performance design and optimization studies. Nonetheless, we want to acknowledge the earlier development work of Biggs and Vittitoe from which this work has evolved.

Caution

The **CIRCE** simulation and subsidiary codes discussed in this report are still in development. While we have performed numerous comparative tests with **HELIOS** and have attempted to insure that all options perform as “advertised”, there may still be “bugs” in the simulation. The authors should be informed if any problems are uncovered during execution of this suite of codes so that future releases will reflect all possible upgrades. Further, the authors would appreciate feedback on this work, especially recommendations for modifications to existing options or for modifications that might serve future needs.

This page is intentionally left blank.

1 Introduction

In this report, a computer simulation code called **CIRCE**¹ is discussed and examples of its application to several concentrating solar collector geometries are presented. **CIRCE**, an acronym for Convolution of Incident Radiation with Concentrator Errors, was developed for the optical analysis of point-focus concentrating dish collector systems. The development of **CIRCE** was predicated on the need for a user-friendly simulation that would provide incident solar flux depositions on flat targets and 2-D axisymmetric cavity and external receivers from continuous- and faceted-reflector systems. Results from such a simulation would be used not only to assess the performance of candidate reflector systems, but also for the design of receiver geometries. Additionally, it was desired that such a simulation be applicable not only on computer systems such as VAX and CDC-mainframes, but also on small personal computers. The latter capability is especially important for eventual dissemination to the developing solar industry.

Development of **CIRCE** was initiated following a review of existing optics simulation codes available for modeling point-focusing collector systems. Candidate simulations included **CAV** [1]², a continuous-surface parabolic dish reflector simulation developed by Ford Aerospace, **COPS** [2], a Monte Carlo simulation developed by Honeywell, and **HELIOS** [3], an optics simulation developed at Sandia National Laboratories, Albuquerque, NM for modeling central receiver-heliostat reflector fields. Of these simulations, the **HELIOS** simulation developed by F. Biggs and C. Vittitoe was best suited for modeling the large variety of reflector and receiver configurations possible for point-focusing solar systems. **HELIOS** is, in theory, capable of modeling any practical reflector and receiver configuration. Realistically, however, using **HELIOS** is difficult since, for most geometries, this would require developing an update file to modify the **HELIOS** source code (which would require a working knowledge of **HELIOS** and in particular, a thorough understanding of the many coordinate frames used throughout the simulation). We chose instead to reconstruct the **HELIOS** simulation to be dish-specific (hence the name, **CIRCE**, who in Greek mythology was the daughter of **HELIOS**) and to provide users with a tool that is relatively easy to implement and does not require a large investment of time to obtain results.

The solution techniques of **CIRCE**, in which the concentrator errors are convolved with the solar intensity profile (sunshape) to produce the flux density distribution on an arbitrary target, are identical to those used in **HELIOS**. **CIRCE** may be used to analyze optical elements that have spherical, parabolic, or no curvature and are either continuous surfaces or faceted. Additionally, facet curvature can be specified using a polynomial fit. This latter option is amenable for modeling stretched membrane concentrator contours. The curvature and aim point of each optical facet comprising the reflector may be individually assigned. The current version of **CIRCE**, referred to

¹In this report, words in uppercase boldface are names of computer simulations or are computer files.

²Numbers in brackets are the references cited in this work and are given in the References Section.

as **CIRCE.001**, is restricted to analyses of reflector systems with flat rectangular or circular targets. Future upgrades will allow two-dimensional axisymmetric external or internal cavity target geometries³ to be analyzed. Currently, user inputs to **CIRCE** include the concentrator geometry, the reflectivity, specularity, slope, and other reflector errors for the optical surface, the collector tracking error, the insolation and sunshape. Output from the code includes a two-dimensional flux density map along the target surface, a “hit” map that indicates the number of facets contributing to the flux at a point on the target, and an overall optical efficiency for the reflector-target system that accounts for possible target shadowing.

CIRCE has been developed with the philosophy that “user-friendliness” is a necessity. To expedite usage of this simulation, we have therefore also developed an interactive data file generator **DEKGEN**, a graphics simulation **PLOT**, which utilizes **DISSPLA** software, and a command procedure file **CIRCE.COM** which executes this suite of codes on a VAX computer system. Additionally, we have modified **CIRCE.001** and **DEKGEN** to execute on IBM-compatible personal computers. For the latter case, a PC command procedure has been developed. Graphics capabilities for the optics simulation have not been completed for PCs, although work on this is in progress.

Important features of **CIRCE** and the subsidiary codes are provided in this report as are several examples of the use of **CIRCE** for optical performance calculations of both faceted and continuous reflector systems. The modeling assumptions and theory used in **CIRCE.001** are the same as those in **HELIOS**; therefore, detailed descriptions of the models are omitted from this report and the appropriate **HELIOS** documentation is instead referenced for review by the reader.

We recommend that the first time user of **CIRCE** read this report in a cursory manner to get an overview of the simulation structure and capabilities. The user may, in fact, prefer to omit the numerical modeling overview (Section 2) initially. The early emphasis should be to review the **CIRCE** Usage Section (Section 7) so that the user will be able to implement the simulation on his particular computer system. Once the **CIRCE** simulation has been installed, the user should attempt to create a data file using **DEKGEN** (preferably modifying the example data files provided on the floppy disks and given in Appendix B). During this execution, Section 4 may need to be reviewed, although all prompts for input in **DEKGEN** should be self-explanatory. Following several executions of the simulation, the user should probably again review the documentation to become more familiar with the different features of **CIRCE** and the background theory. At this time, the user may also want to review the **HELIOS** support documentation referenced in this report.

³Realistic receiver designs for point-focusing concentrators will be internal cavity geometries. External receiver modeling capability is included so that flux spillage on the receiver outer structure can be quantified. This effect may need to be included in receiver thermal analyses.

2 Overview of CIRCE Numerical Modeling

Point-focusing solar collector systems that can be analyzed with **CIRCE.001** consist of two parts, a reflector/concentrator and a receiver/target⁴. Future versions of **CIRCE** may also include a reconcentrator that would be positioned near the focal plane to redirect the solar flux from the reflector to the target. Such a reconcentrator would allow for reducing the aperture area of a cavity receiver and/or “tailoring” the incident flux distribution on the receiver.

The reflector can be constructed as a continuous surface or a number of smaller facets that comprise the reflector geometry. Two very different reflectors that have been in operation and that can be analyzed using **CIRCE** are the LaJet LEC460 solar concentrator used at Solarplant 1 [4], which consists of 24 spherical facets, and the General Electric parabolic dish [5] used at the Shenandoah Georgia solar plant. Photographs of these reflectors are provided in Figures 1 and 2, respectively.

It is assumed in **CIRCE** that the reflector surface is specular, so that the incident and reflected angles for a point on the surface are equivalent within the respective errors associated with the reflector surface. The reflector elements are assumed to be aligned such that the reflected solar flux is directed at particular locations, referred to here as aim points, which can be on or off the target surface. Current reflector contours allowed for in **CIRCE** include spherical, parabolic, and flat surfaces as well as a user-supplied polynomial fit for the facet contour.

Only flat targets, circular or rectangular, can currently be analyzed using **CIRCE**. Flat target modeling capability has been initially emphasized since these targets are useful for assessing the effectiveness of a reflector system for concentrating the solar flux (*i.e.*, reflector optical efficiency). Additional work is currently underway to allow for modeling 2-D axisymmetric internal cavities and external receivers.

In the following subsections, a brief exposure to the modeling theory included in **CIRCE** is provided. The modeling theory incorporated in **CIRCE** is identical to that in **HELIOS**, which has been extensively used to model central receiver solar collector fields. Significantly more detail on the theory is provided in the **HELIOS** reference guide [3], if the reader needs further background.

⁴Throughout this report, the term “collector” is used to denote the reflector and receiver system together. The terms “reflector” and “concentrator” are equivalent as are “target” and “receiver”. A “reconcentrator” is often referred to as a “secondary” or “terminal” concentrator in the literature.

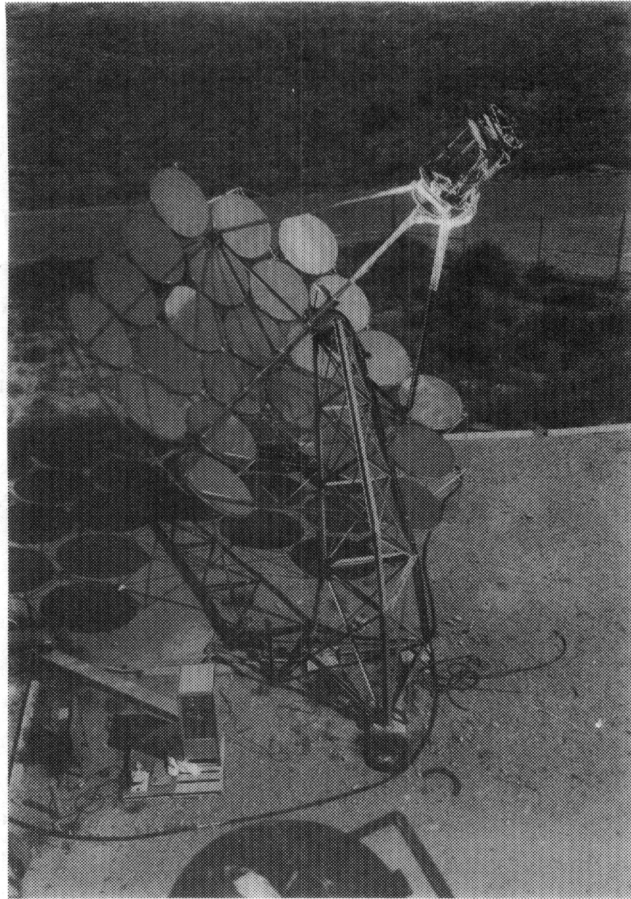


Figure 1: Photograph of a LaJet LEC460 Concentrator located at SNLA.

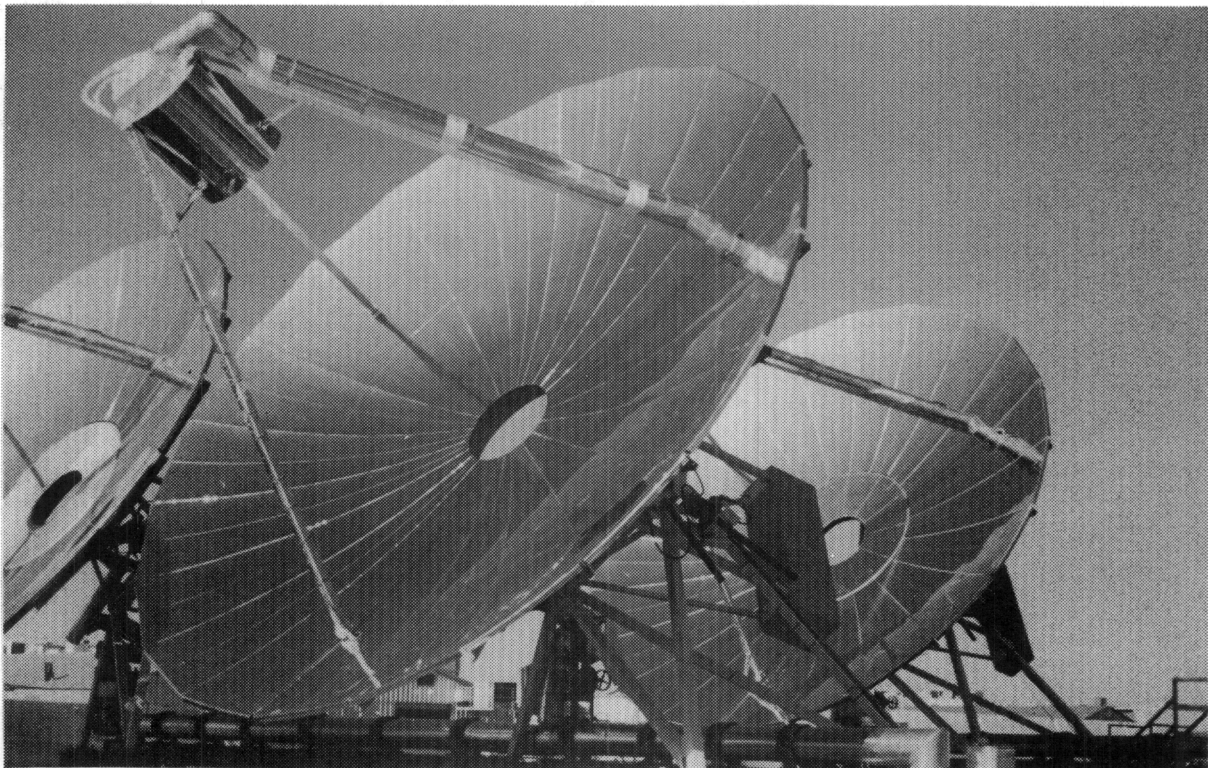


Figure 2: Photograph of the General Electric 7-m parabolic dishes located at Shenandoah, Georgia.

2.1 Incident Flux on Target

The modeling theory of **CIRCE** follows that in the **HELIOS** simulation. That is, the target and reflector are discretized and the flux contribution from each reflector subdivision is computed for each of the target subdivisions. The total flux on the target is then found by integrating the resulting flux profile (map). Figure 3 shows in schematic the reflector-target arrangement as modeled in **CIRCE**. The reflector surface is typically subdivided; the centroid of each “subfacet” comprising the facet or continuous surface reflector is used in the calculations. It is assumed that results calculated for different positions on the subfacet would be the same as the results computed for the subfacet centroid position. It is also assumed that the reflector tracks the sun (so that the sun orientation relative to the reflector is known), and that the reflector and target positions are defined relative to a single coordinate system, so that pertinent angles and distances (slant lengths) can be computed⁵.

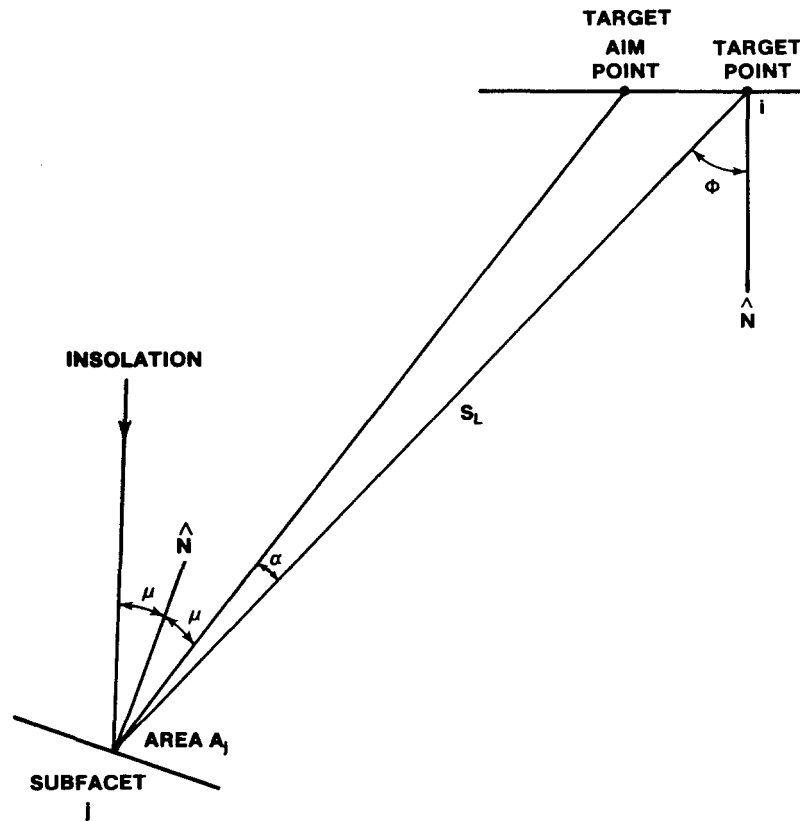


Figure 3: Reflector-target geometry modeled by **CIRCE**.

⁵Data files for **CIRCE** calculations are generated using a single coordinate system with the origin at the vertex of the concentrator. The coordinate system is “right-handed”, with the z-axis vertical, corresponding to dish axis. Although additional coordinate frames are incorporated in **CIRCE**, they are transparent to user. This single coordinate frame is sufficient for defining the solar collector system and for understanding the modeling theory.

The solar flux F_{ij} incident at a target point i (where i is for coordinates x_i, y_i, z_i) from a portion of the reflector (subscript j) is given by Eq.(1). Details on the derivation of this relation are given in References 3 and 6.

$$F_{ij}(x_i, y_i, z_i) = \rho_s A_j (1 - B_j) I D_{ij} \quad (1)$$

where

$$D_{ij} = \left(\frac{\cos \mu_j \cos \phi_i}{S_l^2 \cos^3 \alpha_j} \right) E_{sun}(x_i, y_i, z_i). \quad (2)$$

In Eq.(2), μ_j is the incidence angle for the solar intensity referenced to the local normal of the reflector subfacet, α_j is the angle between the two rays from the subfacet centroid passing through the target aim point and from the subfacet centroid through the target point being analyzed, and ϕ_i is the angle between the target normal and the ray from the subfacet centroid to the target point (These angles are shown in Figure 3). $S_l, I, A_j,$ and ρ_s are the slant distance between the reflector subfacet centroid and the target point, the solar intensity, the subfacet projected area, and the subfacet specular reflectance, respectively. B_j is the target blockage (or shadow) factor, and ranges between zero and unity⁶. The remaining quantity, $E_{sun}(x_i, y_i, z_i)$, is the effective sunshape contribution at the target point. The effective sunshape distribution is computed by convolving the sunshape and the collector error distributions and is described in the following section.

The total flux incident on a target point is computed by summing the contributions from the N_T subfacets, given by Eq.(3).

$$F_i(x_i, y_i, z_i) = \sum_{j=1}^{N_T} F_{ij} \quad (3)$$

Upon completion of these point by point target calculations, the net flux incident on the target is obtained in **CIRCE** by integrating these values numerically. Included are the 9-point integration schemes implemented previously in **HELIOS** [3] and also Legendre-Gauss and Newton-Cotes integration packages. The Legendre-Gauss integrator is used for slowly varying functions (e.g., circumferential variations in the incident fluxes on a circular target), while the more robust Newton-Cotes algorithm is used for integrating rapidly changing flux distributions (as in the radial direction on a circular target). Finally, the optical efficiency for the reflector-target system is obtained from Eq.(4), where again A_j and μ_j are the areas and solar flux incidence angles for each subfacet. The optical efficiency defined in Eq.(4) is the ratio of the integrated flux incident on the target to the total flux incident on the concentrator.

$$\eta_{opt} = \frac{\int_{A_{target}} F dA}{I \sum_{j=1}^{N_T} A_j \cos \mu_j} \quad (4)$$

⁶The shadow factor accounts for the fact that the target, when positioned above the reflector, can block the incident solar radiation from striking part of the reflector. In these situations the solar flux would be incident on the back side of the target. Shadow factors are computed in **CIRCE** by projecting an effective blocking disk of radius r_{shadow} onto the reflector and determining the region of overlap for each facet. Alternatively, target shadow factors can be set to zero or can be assigned by the user.

2.2 Effective Sunshape

In **CIRCE**, the reflected solar intensity is distributed over the target surface. This arises because the sun is treated as a disk, rather than as a point source, and because of reflector and tracking errors. In general, the intensity at a point on the target decreases with increasing distances from the aim point, with E_{sun} depending on the sunshape distribution and on the magnitudes of errors associated with the reflector and tracking. cursory descriptions of the sunshape, of the statistical models for the collector errors, and of the computation of the effective sunshape are provided below. Note that much greater detail is provided in the **HELIOS** reference guide [3].

Sunshape Distribution

The sunshape is assumed to be one-dimensional with the magnitude of the sun's intensity being only a function of the angle with respect to the sun central ray. Sunshape distribution options available in **CIRCE** include "pillbox"⁷, Gaussian, and user-input tabulated distributions. Representative examples are shown in Figure 4.

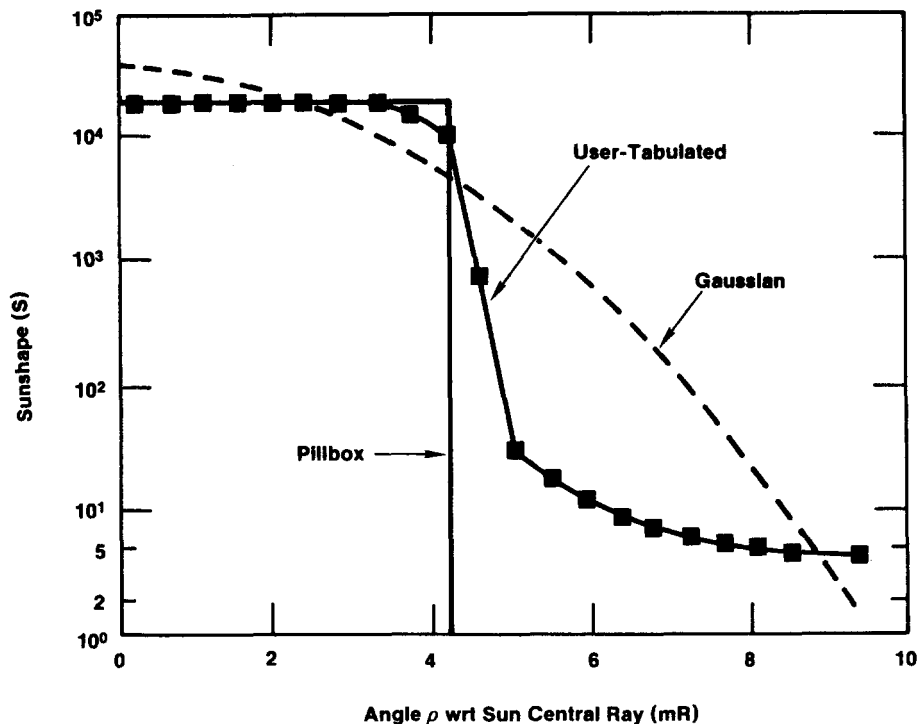


Figure 4: Typical sunshape distributions used in **CIRCE** and **HELIOS**.

⁷ "Pillbox" distributions are sometimes also referred to as "top-hat" functions. In **CIRCE**, six options are provided to smooth the abrupt drop of intensity at the sun edge. These options are discussed in the Sun Parameters section.

The sunshape distribution $\bar{S}(\rho)$ conforms to Eq.(5), where ρ_{edge} is the angle formed by sun central ray and the outer limit of the solar disk beyond which there is no intensity contribution.

$$\int_0^{\rho_{edge}} \bar{S}(\rho) \rho d\rho = 1.0 \quad (5)$$

Note that \bar{S} is the normalized sunshape distribution that is computed internally in **CIRCE** using $S(\rho)$. This distribution can be user-input or is defined internally in **CIRCE** for pillbox or Gaussian sunshapes. Note that this normalization allows for the separation of the magnitude (I), and shape (S) of the insolation distribution.

$$\bar{S}(\rho) = \frac{S(\rho)}{\int_0^{\rho_{edge}} S(\rho) \rho d\rho} \quad (6)$$

Collector Error Distributions

CIRCE allows the user to specify multiple reflector errors (*e.g.*, reflector slope, mirror specularity, random misalignments, etc.,) and vertical and horizontal tracking errors. Reflector and tracking errors are treated statistically yielding elliptic-normal distributions when the errors are 2-D (see Eq.(7)) and reducing to 1-D circular-symmetric distributions (see Eq.(8)) when the errors are 1-D. A 2-D error distribution is specified by the standard deviations, σ_r and σ_s , for the principal axes of the elliptic normal error distribution, for which r and s refer to the major and minor axes, respectively (These axes are related to the x-y dish coordinate frame by the angle θ , which is the angle between the x-axis and the r-axis of the elliptic normal error distribution.). For the 1-D case, $\sigma_t = \sigma_r = \sigma_s$ and the distribution reduces to Eq.(8), where $\bar{r} = \sqrt{r^2 + s^2}$.

$$E_{2D} = \frac{1}{2\pi\sigma_r\sigma_s} \exp\left\{-0.5\left[\frac{r^2}{\sigma_r^2} + \frac{s^2}{\sigma_s^2}\right]\right\} \quad (7)$$

$$E_{1D} = \frac{1}{2\pi\sigma_t^2} \exp\left\{-\frac{\bar{r}^2}{2\sigma_t^2}\right\} \quad (8)$$

Since all errors are analytical distributions, they can be convolved analytically to obtain a single effective elliptical normal error distribution. When the errors are 1-D, the effective error (σ_t) reduces to the root-mean-square of the K_i individual errors as given by Eq.(9).

$$\sigma_t = \sqrt{\sum_{k=1}^{K_i} \sigma_k^2} \quad (9)$$

It is important that the reader realize that all reflector errors are treated in **CIRCE** as if they were slope errors. That is, all errors are defined as the difference between the actual surface normal and the theoretical “perfect” surface normal. This is different from tracking and specular errors, which are more typically defined between a point sun source and the reflected ray. Since the factor of two associated with the slope error is “hardwired” in **CIRCE**, the user must accordingly reduce the magnitude of non-slope errors such as specular or random misalignment. As an example, if the specular error is to be 1.5 mR for a reflector, then the error should be input as 0.75 mR, since the error will be doubled during **CIRCE** execution. Note also that the statistical treatment of tracking errors is the same as for reflector errors such as slope or specular errors. When tracking errors are convolved with the reflector errors to create the total error distribution, the resulting distribution should be interpreted as the time-averaged probable error distribution which would occur for a reflector with an incremental tracking system. Tracking errors should not be included in Eq.(9) when instantaneous results are desired.

Convolution of Sunshape and Error Distributions

The effective sunshape distribution E_{sun} is obtained by convolution of the normalized sunshape \bar{S} with the reflector and tracking errors [3]; this resulting intensity distribution can be 1-D or 2-D, depending upon the dimensionality of the errors. As in **HELIOS**, the convolution of the sunshape with the elliptic normal error distributions can be accomplished analytically or numerically (using fast Fourier transforms). In **CIRCE**, it is assumed that the effective sunshape distribution is the same for all positions on the concentrator and is computed for the the first subfacet centroid position.

Convolution of the sunshape and error distributions yields an effective sunshape which is described mathematically in terms of coordinates in the reflected-ray reference plane (referred to as the U-V plane in the **HELIOS** reference report) shown in Figure 5. This reference plane is perpendicular to \hat{B}_0 , which is the unit vector for the ray from the subfacet centroid to the target aim point. Similarly, \hat{B} and \hat{C} are unit vectors from the subfacet centroid to the target point, and the projection of unit vector \hat{B} in the y-z plane, respectively.

The effective sunshape magnitude E_{sun} at target point P is defined in the reflected-ray reference plane at point Q shown in Figure 5. For 2-D distributions, E_{sun} is quantified in terms of the components U and V . Relations for the magnitudes of these components in the x, y, z coordinate frame are derived in the **HELIOS** reference guide [3]. Equations (10) and (11) shown below express these quantities in terms of the unit vectors shown in Figure 5⁸

$$U = \frac{\sqrt{1 - (\hat{B} \cdot \hat{C})^2}}{(\hat{B}_0 \cdot \hat{B})} \quad (10)$$

⁸The U expression has been corrected from that in the **HELIOS** reference guide.[3]

$$V = \frac{\sqrt{1 - (\hat{B}_0 \cdot \hat{C})^2}}{(\hat{B}_0 \cdot \hat{C})} \quad (11)$$

For 1-D circular symmetric distributions, E_{sun} is a function only of $\rho = \tan\alpha$. The reader is referred to the **HELIOS** reference report for additional details pertaining to the effective sunshape.

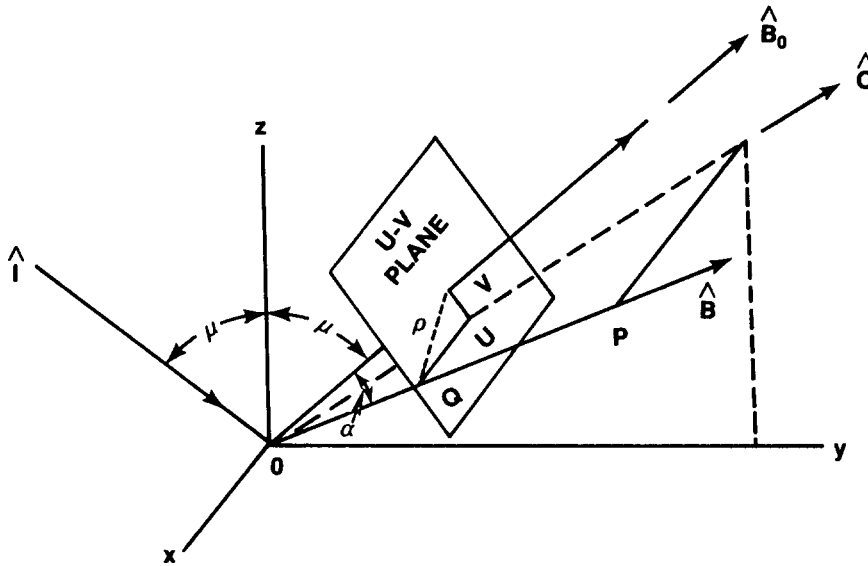


Figure 5: Geometry of target point P and the reflected-ray reference plane.

3 CIRCE Structure

CIRCE was developed for analyzing/designing point-focus solar collectors. Although much of **CIRCE** is taken directly from **HELIOS**, the structure of the code is somewhat different. **HELIOS** was developed using an overlay structure compatible with the CDC NOS operating system used at SNLA. This structure has been eliminated in **CIRCE**, thereby eliminating large quantities of redundant source code. Additionally, the central receiver options included in **HELIOS** have been eliminated, since **CIRCE** is a “dish specific” simulation. Many other **HELIOS** options were also omitted to reduce the size of the simulation when it was felt that the options were either not needed (*e.g.*, atmospheric attenuation models) or were redundant (*e.g.*, sunshapes that could be specified using the tabular option).

As opposed to **HELIOS**, **CIRCE** is a “stand-alone” simulation. Although **HELIOS** provides most, if not all, options pertinent to central receiver applications, the user must supply subroutines or alter the source code via updates for a significant number of dish applications. We have included a sufficient number of target, reflector, and sunshape options such that **CIRCE** should not need to be modified by the user. In addition, work is underway to incorporate options such as internal and external receiver geometries and reconcentrators to make **CIRCE** more useful for dish modeling.

The **CIRCE** execution sequence is summarized below:

1. Read data file and compute reflector and target orientation based on sun position
(Developed from **HELIOS** Overlay 1,0 – Program A)
2. Compute target blockage factors if required
(Developed from **HELIOS** Overlay 2,0 – Program B)
3. Compute sunshape distribution
(Developed from **HELIOS** Overlay 5,0 – Program D)
4. Compute effective sunshape distribution
(Developed from **HELIOS** Overlay 3,0 – Program C)
5. Perform facet to target point incident flux calculations for N_T subfacets
(Developed from **HELIOS** Overlay 3,0 – Program C)
6. Integrate flux distribution on the target and compute optical efficiency
(Developed from **HELIOS** Overlay 3,0 – Program C)

Since the basic **HELIOS** framework has been maintained where possible, we have indicated the particular **HELIOS** overlays from which the **CIRCE** calculation sequences were developed. Flowcharts for the **HELIOS** overlays are provided in Reference 7 and additional support documentation is provided in Reference 8.

4 Data File Generation

Utilization of the **CIRCE** simulation is facilitated by **DEKGEN**, which is an interactive data file generation code. **DEKGEN** produces a data file that consists of the four data groups given below:

- General problem parameters
- Sun and error parameters
- Target/receiver parameters
- Reflector/facet parameters

The structure of a **CIRCE** data file was taken from the structure required for **HELIOS** data files, described in Reference 7, but is considerably different. We have greatly reduced the quantity of parameters and have streamlined the data file structure from the eight data group format required by **HELIOS**. Additionally, the data files are read by **CIRCE** using a free-format structure, as opposed to the fixed-format structure of **HELIOS**. The free-format structure allows the user to easily modify existing data files. Most importantly, we have made it easier for the user to supply coordinate locations for the reflector facets and the target plane because a single “right-handed” coordinate system is used. The origin of this system corresponds to the dish vertex and the z -axis corresponds to the axis of the dish reflector. Figure 6 shows a typical reflector/target system in the dish coordinate frame used in **CIRCE**. This coordinate frame is comparable to the facet coordinate frame used in **HELIOS**. Since many of the coordinate frames of **HELIOS** still remain in **CIRCE**, we have included the appropriate transformations from the “dish” coordinate frame to the appropriate **HELIOS** coordinate frames.

DEKGEN can be used to create a new data file, or can be used to modify a previously generated data file. When the latter option is specified, **DEKGEN** accesses the previously created file, and displays the current values for the parameters from each data group prompting the user as to whether any of the parameters from that group are to be altered. If one parameter is to be altered, then all parameters from that data group must be redefined (input). Additionally, **DEKGEN** allows the user to access previously generated files containing sunshape data and reflector geometry data that can be quite lengthy. These options are intended to simplify the data generation procedure.

In general, the creation of a **CIRCE** data file using **DEKGEN** is straightforward and the user should not need any support documentation to understand the prompts provided during a data file generation session. **DEKGEN** writes to the computer monitor the variable definitions and options, and then prompts for the parameter. For many variables, default options are suggested. Logic internal to **DEKGEN** is used to simplify the data input so that the number of prompts is minimized. Finally, the

user is offered detailed or cursory variable description options. For first time users of **DEKGEN**, detailed descriptions are provided; on the other hand, experienced users will appreciate the brevity of the cursory variable prompts. Given that the prompt descriptions can be reduced and that existing files can be used during a data file generation, we recommend that **DEKGEN** be used to edit an existing data file until the user is quite familiar with the data file parameters and structure.

Data files for **CIRCE** consist of four parts as indicated above, with a user-input title initiating each part. The general problem parameter title should be used as a descriptor for the entire data set, while the other three descriptors are useful for defining the specific reflector and receiver geometries and the sun data. These latter descriptors are prompted for upon completion of the generation of the particular data group, rather than at the start, so that the user can create a descriptor representative for his answers to the **DEKGEN** prompts. Below, additional descriptions of the variables of each data group are provided. We have also tabulated the variable names used in **DEKGEN**, as well as providing a brief description of the variables and the appropriate units to be used, in Appendix A.

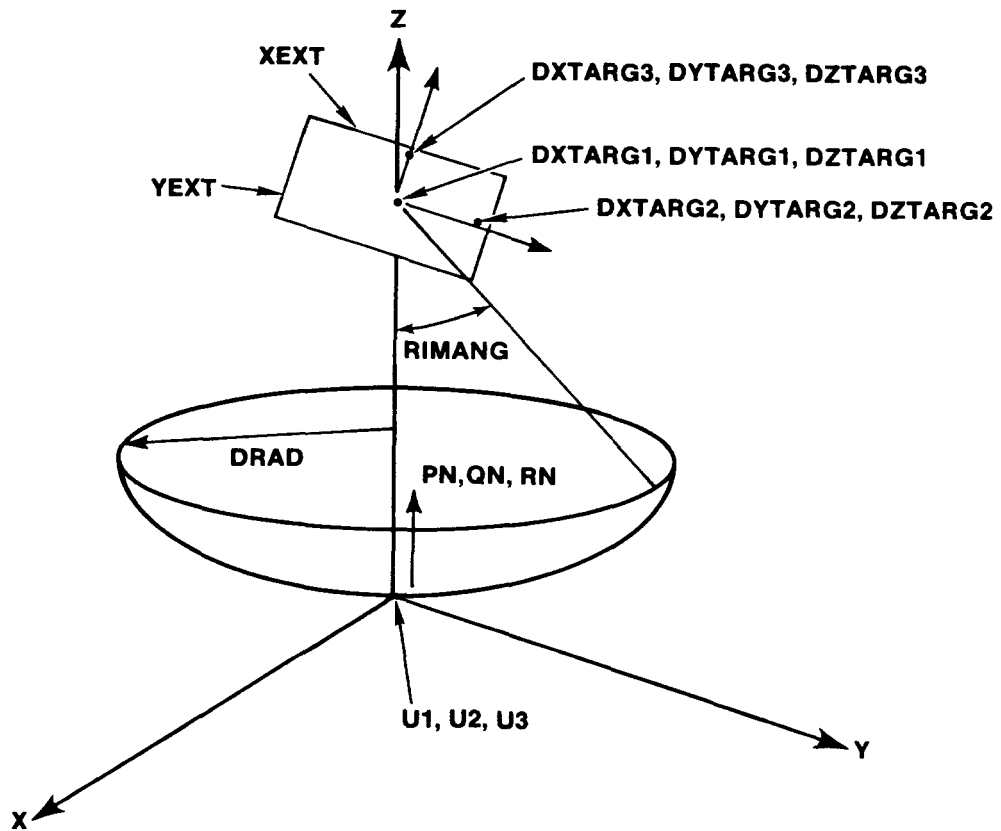


Figure 6: Schematic of a concentrator/target in the dish coordinate system used in the **CIRCE** simulation. Variables shown in figure are same as used in **DEKGEN**.

4.1 General Problem Parameters

The general problem parameters include output options for printing (IPRINT⁹) and plotting (IPLOT), as well as parameters defining the time of day (SOLTIM), day of year (SDAY), and latitude (PHIL) for the solar collector. The latter parameters are used to define the sun position and to orient the solar collector. Since it is assumed that the reflector is oriented so that the projected reflector surface is perpendicular to the sun central ray (*i.e.*, on-axis tracking) subject to tracking errors, these data are not critical to the analyses; default options of SOLTIM=0, SDAY=80, and PHIL=34.96 are used unless otherwise specified.

The IPRINT = 0 option is the normal output mode; IPRINT=1 allows for additional output for flux contributions from each facet for 5 or less target points. When IPLOT=1, output for later plotting is saved; for IPLOT=0, a null file is generated.

4.2 Sun and Error Parameters

Sunshape Definition

The solar intensity distribution is defined by the insolation level (SI) and the sunshape. As indicated previously, the sunshape $S(\rho)$ is assumed to be one-dimensional. Three options are available for the sunshape type (defined by JSUN). The sunshape can be user tabulated (JSUN=1), Gaussian, (JSUN=2) or a “pillbox” distribution (JSUN=3). For the pillbox distribution, one of 6 smooth-down options (IDL) for the limb (end of) of the distribution can be chosen. In addition, the user must specify the start of the limb α (ALO) and the end of the limb β (BLIM). Available limb profiles $L(\rho)$, where ρ is the angle measured with respect to the sun central ray and $\alpha \leq \rho \leq \beta$, are given below. Figure 7 shows these different limb decay options, assuming that the start and end of the limb correspond to 4.6 and 5.6 milliradians, respectively.

Cosine decay (IDL=1):

$$L(\rho) = 0.5 \left(1 + \cos \pi \left[\frac{\tan \rho - \tan \alpha}{\tan \beta - \tan \alpha} \right] \right) \quad (12)$$

Gaussian decay (IDL=2):

$$L(\rho) = \exp \left(-5 \left[\frac{\tan \rho - \tan \alpha}{\tan \beta - \tan \alpha} \right]^2 \right) \quad (13)$$

Linear decay (IDL=3):

$$L(\rho) = \frac{\tan \beta - \tan \rho}{\tan \beta - \tan \alpha} \quad (14)$$

No decay until end of limb (IDL=4):

$$L(\rho) = 1.0 \text{ for } \alpha \leq \rho < \beta; \quad L(\rho) = 0 \text{ for } \rho \geq \beta \quad (15)$$

⁹Variable names listed in this report are the same as used in **DEKGEN** and are capitalized.

No Limb (IDL=5):

$$L(\rho) = 0 \text{ for } \rho > \alpha \quad (16)$$

Exponential decay (IDL=6):

$$L(\rho) = \exp\left(-5 \left[\frac{\tan \rho - \tan \alpha}{\tan \beta - \tan \alpha} \right]\right) \quad (17)$$

When JSUN=1, the user must provide a sunshape distribution as a function of increasing angle ρ from the sun central ray ($\rho = 0$). If the selected sunshape is to be Gaussian, the user must provide α (ALO) which corresponds to the edge of a uniform sun disk and is used to generate a Gaussian distribution with an equivalent rms width. Additionally, the cutoff for the Gaussian distribution β (BLIM) must be specified. The Gaussian distribution is given by:

$$S(\rho) = \exp\left(-5 \left[\frac{\tan \rho - \tan \alpha}{\tan \beta - \tan \alpha} \right]^2\right) \quad (18)$$

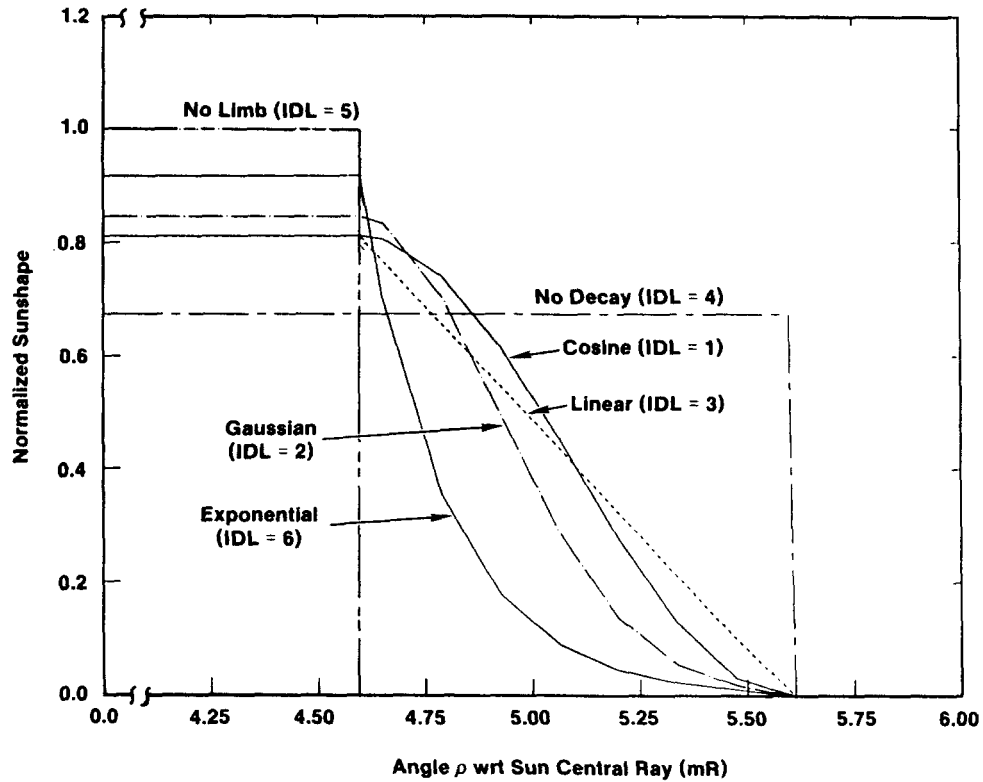


Figure 7: Six limb options for pillbox sun. The sunshape magnitudes here have been normalized using the “no limb” normalized sunshape magnitude \bar{S} .

Error Definition

Reflector errors are specified as area-averaged and tracking errors as time-averaged normal error standard deviations between the surface normal and the theoretical “perfect” surface normal (refer to Section 2.2 for more detail). Up to 5 reflector errors ($0 \leq \text{NER} \leq 5$), such as slope and specular errors, can be handled by **CIRCE**. Since all errors are treated as slope errors in **CIRCE**, the user should reduce non-slope errors by a factor of two when the errors are input. As an example, a slope error of 2.5 mR would be input as 2.5 mR, while a specular error of 3.0 mR would be input as 1.5 mR. It is also assumed that all errors conform to an elliptic normal distribution. Reflector errors are specified by the standard deviations for the major and minor axes (SIGX and SIGY in milliradians¹⁰) of the elliptic normal distribution; these axes need not correspond to the x and y axes of the dish coordinate frame but can be offset from the x-axis by some rotation angle θ (TH in degrees).

Tracking errors are defined as the standard deviations of 1-D normal distributions describing the accuracy of tracking along the horizontal elevation axis (TRH) and the vertical azimuthal tracking axis (TRV). For situations where the user does not wish to model reflector errors (NER=0) and where he assigns no tracking errors (NTR=0), **DEKGEN** will assign an arbitrarily small 1-D reflector error of 0.01 milliradians. This is required so that the effective sunshape can be computed by **CIRCE**.

Convolution of Sunshape and Errors

CIRCE convolves 2-D errors with 1-D sunshapes to create either a 1-D (IDIM=1) or 2-D (IDIM=2) effective sunshape. The convolutions can be performed numerically (IANLYT=0) using fast Fourier transforms or analytically (IANLYT=1). When the user chooses to perform the convolution analytically, the sunshape is represented as a Gaussian distribution with the same rms width as for the input sunshape. IANLYT and IDIM default to unity for situations where the sunshape is Gaussian (JSUN=2) and the errors are 1-D, respectively. When **CIRCE** is executed on PCs, the analytical convolution and 1-D effective sunshape options should be used where possible since execution time is reduced for these choices.

4.3 Target/Receiver Parameters

Target/receiver parameters are required for the definition of flat targets that are presently limited to be either rectangular (ITARSH=0) or circular (ITARSH=1). The size of a rectangular target is defined in terms of extents on each side (XEXT, YEXT); for the purpose of computing an accurate flux distribution, the rectangular target can be divided into as many as 121 parts, using 11 equal subdivisions (IXPTS, IYPTS)

¹⁰SIGX and SIGY are input during **DEKGEN** execution as milliradian errors and are written to the .DAT file as radian errors. Similarly, the user is prompted by **DEKGEN** to provide the solar intensity SI in units of W/m² and this value is modified to be in units of W/cm² in the .DAT file. Refer to Appendix B for examples of **DEKGEN**-generated data files.

in each direction. When the target is circular, the target radius (XEXT) must be specified. Circumferential subdivision of circular targets (IYPTS) is to be ≤ 11 equal increments, while the target can be divided into 51 or fewer equal radial increments (IXPTS).

Note that if circumferential symmetry is expected, the user can reduce his execution time significantly by modeling a circular target with IYPTS=1¹¹, corresponding to $\Delta\theta = 2\pi$. Additionally, the circular target should be selected if the user wants to compute the collector optical efficiency as a function of radial distance. When the target is circular, the optical efficiency is computed using Eq.(4), with the target area conforming to some delta area, *i.e.*, area for a ring of the target disk from r_i to r_{i+1} , with i incremented from 1-IXPTS. These contributions are summed ($\eta_{r_k} = \sum_{i=0}^k \eta_i$) to compute the overall optical efficiency. For rectangular targets, only the overall optical efficiency is computed.

The target position and orientation are defined with respect to the reflector coordinate system, with the reflector center assumed to be positioned at the coordinate frame origin. The target orientation is defined by three noncolinear points (DXTARGI, DYTARGI, DZTARGI, I=1,3) in the target plane. The center of the target (DXTARG1, DYTARG1, DZTARG1) must be input. For reflectors that can be modeled as effective parabolic dishes, **DEKGEN** will compute the effective focal length, given the dish radius r_{dish} and rim angle η ¹² as shown below; this is useful for defining DZTARG1.

$$f = 0.5r_{dish} \left(\tan^{-1}\eta + \sqrt{\tan^{-2}\eta + 1} \right) \quad (19)$$

When the target is aligned so that the target plane is perpendicular to the central sun ray (normal target alignment), then two additional points in the target plane are automatically generated by **DEKGEN**. For a canted target alignment, the user must specify the other two target points in the canted target plane. The user must also specify the number of aim points (NFOC) for the reflector in the target parameters data group. At present, NFOC must be 5 or less. These aim points are defined according to the dish coordinate frame; each aim point is assigned an integer identifier (sequential identifier from I=1,NFOC) that is used in the reflector data group for assigning the aim point for each facet.

Two additional data items are required in this data group. The first parameter allows the user to specify whether target shadowing of the reflector is to be accounted for, using the integer flag ISHAD. For ISHAD=0, target shadowing is omitted, while for

¹¹As indicated in Section 2.1, we have included the **HELIOS** integration schemes and also an improved integration algorithm for computing the incident power on the target. The target flux integration schemes taken from **HELIOS** require that IXPTS and IYPTS be 3 or greater. For IXPTS and IYPTS less than 3, only the Legendre-Gauss and Newton-Cotes integration schemes added to **CIRCE** are used.

¹²The rim angle is the angle formed between the rays from the focal point to the dish vertex and to the edge of the parabolic dish. Alternatively, parabolic dishes are often defined by f/d ratios, where $d = 2r_{dish}$; for these cases $\tan\eta = \frac{8f/d}{(4f/d)^2 - 1}$.

ISHAD=1, shadow factors are computed internally by **CIRCE**. For this latter option, the user must specify an effective target shadow radius (SHADR). Additionally, for ISHAD=2, the user can specify that target shadow is to be accounted for, with the factors user-provided. For this case, the shadow factors are specified for each facet in the reflector/facet data group. The second set of prompts occur if the extensive printout option IPRINT=1 was assigned in the general problem parameter group. For this case, the user can specify 5 or less target points for which facet flux contributions will be provided and can also specify a single target point (NTAGP) for which D_{ij} , defined by Eq.(2), will be provided for every subfacet. These latter options are useful for assessing which facets are reflecting solar flux to particular target locations. Note that the prompts for these detailed output options call for the target point integer designators rather than the target point location. These designators are provided in the extensive **CIRCE** output file (see Section 5); we recommend that a **CIRCE** simulation should first be performed with IPRINT=0. The user can review his results and select appropriate target points prior to re-executing **CIRCE** using IPRINT=1.

4.4 Reflector/Facet Parameters

CIRCE can be used to model either continuous-surface reflectors or reflectors comprised of individual facets. The VAX version of **CIRCE** is capable of modeling up to 250 facets (NFACET), whereas the PC version is limited to 50 facets because of storage limitations. It is assumed that the facets are specular reflectors. The effective specular reflectance ρ_s (REFLEC) for the reflector is a user input.

Facets are described by their projected shape and contour. **CIRCE** can be used to model circular (KORD=1) and rectangular facets (KORD=2). When a reflector consists of two or more facets, all facets are assumed to have the same area. When the facets are rectangular, the extents must be specified (ELENX, ELENY); for circular facets, the radius (FLENG) is required. Each facet can also be subdivided. The extents ELENX and ELENY can be divided into NX and NY parts, respectively, for rectangular facets, while for circular facets, FLENG can be divided into NSUBF equal radial increments. **CIRCE** will automatically subdivide the circular facet circumferentially, so that the subfacets will have comparable areas. Note that while there is no imposed limit on the number of subfacets that can be used, the total will seriously affect **CIRCE** execution time. In general, the execution time is proportional to the total number of subfacets $N_T = \text{NFACET} \times N_F$, where $N_F = \text{NX} \times \text{NY}$ for rectangular facets and is a function of NSUBF for circular facets. Table 1 shown below gives an estimate of typical N_F for different NSUBF, as computed for a 7-m radius 45° parabolic dish (see Example 1 of Section 6 for details on the dish).

Table 1: Reflector Subfacets as a Function of Radial Subdivisions

Radial Subdivisions NSUBF	Total Subfacets N_F
3	26
5	77
7	154
10	315
15	710
20	1263
25	1972
30	2839

Contours presently available include parabolic (IOPT=1), flat (IOPT=2), spherical (IOPT=3), and a user specified polynomial fit (IOPT=4). When the facets are parabolic, the focal length for each facet must be input, while for spherical facets, radii of curvature are required. The user must specify some default curvature for flat facets although this input is not used during **CIRCE** execution.

The fourth reflector curvature option (IOPT=4) has been included for the purposes of evaluating innovative concentrators such as stretched membrane reflectors. This option allows the user to input the facet contour using a power series of the following form:

$$Z(R) = \sum_{k=1}^K A_k R^{k-1}, \quad 0 \leq K \leq 10. \quad (20)$$

It is assumed that the Z -displacement is a function of the radial position as measured from the facet center¹³. The coefficients A_k may be known *a priori* or can be obtained from a least squares fit of displacement data measured for a concentrator.

Within **CIRCE**, the position on the facet and also the normal vector at that position are needed to compute the energy incident on the target from different concentrator locations. The unit normal vector ($\hat{N}_x, \hat{N}_y, \hat{N}_z$) for any position on the concentrator is given by Eqs.(21–23). These relations were developed from the more general relations provided in Reference 6.

$$\hat{N}_x = -BX/C \quad (21)$$

¹³This formulation is valid for concentrators with circular projections and can also be used to model rectangular facets. In the computation of the energy incident at the target from each subfacet centroid, the centroid is defined in a Cartesian coordinate frame. The facet curvature and also the normal components at the centroid are computed as functions of R , where $R = (X^2 + Y^2)^{0.5}$.

$$\hat{N}_y = -BY/C \quad (22)$$

$$\hat{N}_z = 1.0/C \quad (23)$$

where,

$$B = \sum_{k=2}^K (k-1)A_k R^{k-3} \quad (24)$$

and

$$C = \sqrt{1.0 + B^2(X^2 + Y^2)}. \quad (25)$$

Results using the polynomial fit contour option have been compared with results computed for spherical (IOPT=3) and parabolic (IOPT=1) facets. For parabolic facets, the displacement is given by:

$$Z = \frac{1}{4f} R^2, \quad (26)$$

where f is the focal length. Results from **CIRCE** executions using the power series relation (denoted by IOPT=4) and the built-in option for parabolic contours (IOPT=1) are identical, as would be expected. For the spherical contour option, we have computed the Z -displacements for a 7-m radius dish with an f/d of unity and performed a least squares curve fit generating 2 representative displacement relations given below:

$$Z(R) = 1.01094(10^{-3}) - 1.83299(10^{-3})R + 1.83601(10^{-2})R^2 \quad (27)$$

$$Z(R) = 1.22768(10^{-6}) - 2.12534(10^{-5})R + 1.78794(10^{-2})R^2 \\ - 7.45046(10^{-6})R^3 + 6.55119(10^{-6})R^4. \quad (28)$$

Computed heat flux magnitudes at representative radial positions distributions on a circular target are provided in Table 2 comparing results from second and fourth order polynomial fits for the curvature with results computed using the spherical contour option (IOPT=3) in **CIRCE**. As is apparent, good agreement is possible if the fourth order polynomial fit is used. That the second order fit is less accurate should indicate the importance of determining an accurate functional relation for the concentrator shape.

The reflector geometry is defined using the dish coordinate system, where it is assumed that the dish vertex is at the coordinate frame origin. Each facet center must be input; **CIRCE** will perform computations for each subfacet centroid position needed in Eqs.(1-2). Additionally, the user can either input each facet normal (ICPQR=1) or the normals can be computed by **CIRCE** (ICPQR=0). If the user chooses to input his own normals, he may either interactively input the facet identifier (IDF) and the

vector components (PN, QN, RN) or may generate a free-formatted data file prior to **DEKGEN** execution which can be accessed by **DEKGEN**. Note that for this option (ICPQR=1), aim points are not used in the analyses, since the facet orientation is defined by the normal vector. When the normals are computed internally in **CIRCE**, (ICPQR=0), the facet center locations, the sun position, and the aim points are used to orient the facet.

When more than one aim point (NFOC>1) is defined in the target data group, then an aim point integer identifier must be assigned to each facet. Similarly, if ISHAD=2, the user must provide blockage factors for each facet. When a reflector consists of many facets, it may be beneficial to assemble a free-formatted facet geometry file prior to executing **DEKGEN**. This file would include: the facet number (IDF), the x,y,z coordinates of the facet center (U1,U2,U3), the facet focal length or radius of curvature (FOC), the blockage factor (SBM), and the aim point identifier (NFID). **DEKGEN** will access this data file, simplifying the data file generation process.

Table 2: Heat Flux Distributions – Polynomial Fits Compared with Spherical Curvature Results

Radial Position (m)	Incident Heat Flux (W/cm ²)		
	Spherical (IOPT=3)	2nd Order (IOPT=4)	4th Order (IOPT=4)
0.000	1.688E+02	1.770E+02	1.687E+02
0.030	1.626E+02	1.709E+02	1.625E+02
0.060	1.456E+02	1.540E+02	1.455E+02
0.090	1.217E+02	1.296E+02	1.216E+02
0.120	9.548E+01	1.023E+02	9.547E+01
0.240	2.344E+01	2.239E+01	2.348E+01
0.360	3.803E+00	2.160E+00	3.816E+00
0.480	3.190E-01	8.746E-02	3.207E-01
0.600	1.012E-02	1.262E-03	1.017E-02
0.720	9.820E-05	0.000E+00	9.891E-05

5 CIRCE Output

Results from **CIRCE.001** execution are provided in two output files, **FILE.FLX** and **FILE.OUT**, where “FILE” is a user-specified filename¹⁴. **FILE.OUT** is the extensive output file generated by **CIRCE**, while **FILE.FLX** is a summary file which includes sunshape and flux distributions. When **CIRCE.001** is executed on the SNLA VAX computer systems, **FILE.FLX** can be accessed to generate graphical output if desired, and these results are written to **FILE.PLT**. **FILE.PLT** is created using a graphics computer simulation **PLOT** which utilizes the ISSCO proprietary **DISSPLA** plotting software [8] with the Sandia virtual device interface (VDI).

Additional information on these output files is given below.

FILE.OUT

FILE.OUT is the extensive output file generated by **CIRCE**. It includes:

- Definition of the input parameters from the data file
- Sun angles and associated reflector and target orientation relative to the sun
- Computed facet shadow factors (if required)
- Sunshape distribution
- Convolved sunshape and error distribution
- Flux contributions to particular target locations from all facets (if extensive output options are specified)
- Incident flux distributions and “hit” map for the target
- Collector optical efficiency

The geometry for the **CIRCE** analyses is transformed from the dish coordinate frame used in the data file generation to the different coordinate frames used in **HELIOS** (*e.g.*, tower coordinate, heliostat coordinate, and sun coordinate systems). For details on these coordinate frames, the user should review the **HELIOS** reference guide [3]. In particular, the output for the incident flux distribution and for the hit map¹⁵

¹⁴The command procedures developed for executing the **CIRCE** optics package rename the output files using .OUT, .FLX, and .PLT identifiers (the .PLT file is currently generated only during VAX execution). The user also must specify a filename, referred to as “FILE” in this text, which is used to identify the output from a given execution of the optics package.

¹⁵The “hit” map provides a count of the number of subfacets which “contribute” to the flux at the individual target points. A subfacet is assumed to contribute flux if F_{ij} computed using Eq.(1) is nonzero. The “hit” map is intended only to provide qualitative information pertaining to the flux distribution.

are given using the target coordinate system, whose origin is at the target center. This reference coordinate frame has been maintained in **CIRCE** since we intend to use this system for performing receiver heat transfer studies; output and geometry based on this coordinate frame will need to be used in receiver heat transfer simulations.

FILE.FLX

FILE.FLX contains summary results from **CIRCE.001** execution. Included are:

- 1-D sunshape distribution
- Convolved sunshape and error distribution
- Incident flux distribution on target
- "Hit" map for target
- Optical efficiency distribution if the target is circular

Title descriptors are provided for each of these distributions. Additionally, parameters (such as row and column magnitudes), needed for executing **PLOT** on the VAX computer system, are included in **FILE.FLX**.

FILE.PLT

FILE.PLT is a binary plot file generated using the **DISSPLA** plotting software available to SNLA. Graphical output is generated by a graphics program **PLOT**, which produces plots using **FILE.FLX** data. At present, graphical output written to **FILE.PLT** can be disposed (*i.e.*, printed on) to Versatec printers or QMS output devices. Graphical results from **FILE.PLT** are provided in the following section.

6 Illustrative Examples

In this section, results are presented that illustrate some of the more important capabilities of the CIRCE simulation. These examples include:

- Comparisons of different spherical and parabolic dish geometries
- Comparison of a three facet dish with a single facet dish
- Test Bed Concentrator #1 (TBC-1) performance

In the first example, comparisons of the performances of several continuous-surfaced spherical and parabolic reflectors are provided. In the second example, results from a reflector composed of 3 facets (spherical and parabolic) are compared with single continuous spherical and parabolic concentrators. In the third example, the TBC-1 reflector at SNLA [10], which consists of 220 rectangular facets, is modeled¹⁶. Here, results are presented for the reflector as it is nominally configured (*i.e.*, a single aim point and three radii of curvature for the different facets), along with results for multiple aim points and for different facet radii of curvature conditions.

For comparison, sun and error parameters have been held constant for each of these examples. The nominal reflector and tracking errors are given below, and the tabular sun distribution shown previously in Figure 4 is used. The errors are convolved with the sunshape yielding an effective 1-D sunshape given in Figure 8.

Table 3: Reflector and Tracking Error Budget

Error	Magnitude [†]
1-D Reflector Slope Error	2.5
1-D Mirror Specularity	1.5
Horizontal Tracking Error	1.2
Vertical Tracking Error	1.2

[†] Errors in milliradians as input to **CIRCE**

For these studies, it is also assumed that the facet reflectivity ρ_s is unity, and that the target does not shadow the reflector (ISHAD=0). These constraints are imposed so that the reflector optical efficiency η_{opt} will be unity for sufficiently large targets, rather than:

$$\eta_{opt} = \rho_s \frac{\sum_{j=1}^N A_j (1 - B_j)}{\sum_{j=1}^N A_j},$$

where A_j is the projected area of each facet.

¹⁶We also expect to model the TBC-1 reflector to compare with flux maps measured at the SNLA STTF. To date, these measurements have not been completed.

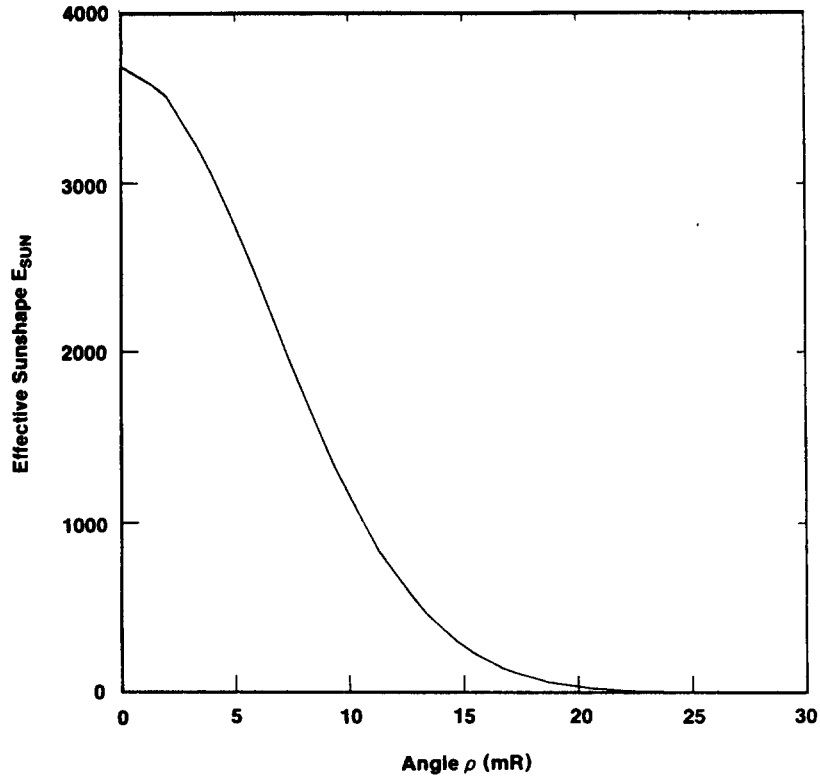


Figure 8: 1-D effective sunshape used in examples. This distribution represents the convolution of the tabular sunshape of Figure 4 with errors summarized in Table 3.

6.1 Example 1: Spherical and Parabolic Dishes

In this example, results are provided for different contoured parabolic and spherical dishes, all of which are 14.0 m in diameter. Three parabolic dishes with $f/d = 0.43$, 0.60, and 0.93 are considered, (dish rim angles of 60° , 45° , and 30° , respectively); for comparison, three spherical dishes having $f/d = 0.6$, 0.8, and 1.0 are also modeled (The radii of curvature for the spherical dishes $\mathcal{R} = 2f$). Circular targets are modeled, each centered at the dish aim points $(0,0,f)$. Incident heat flux and optical efficiency results are given as a function of radial position on the circular targets in Figure 9 for the parabolic dishes and in Figure 10 for the spherical dishes, respectively.

Results for these different reflectors are as expected. In all cases the overall collector optical efficiency approaches unity as the target size is increased. For the parabolic dishes, the size of the target must be increased with increasing f/d to capture all of the reflected energy. The peak incident flux density at the target center falls off with increasing f/d for the parabolic dishes, which would be expected, since the slant lengths are so much greater. Since we have assumed in these calculations that the error budgets for each parabolic dish are the same, the trends reported here for parabolic dishes may be somewhat misleading. In particular, the slope error might be expected to increase as f/d is decreased, since it would be more difficult to maintain the parabolic shape.

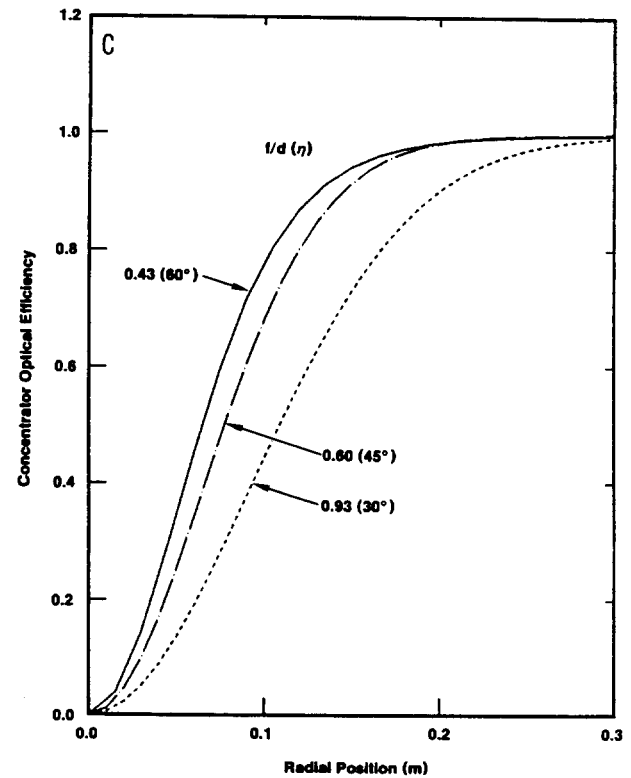
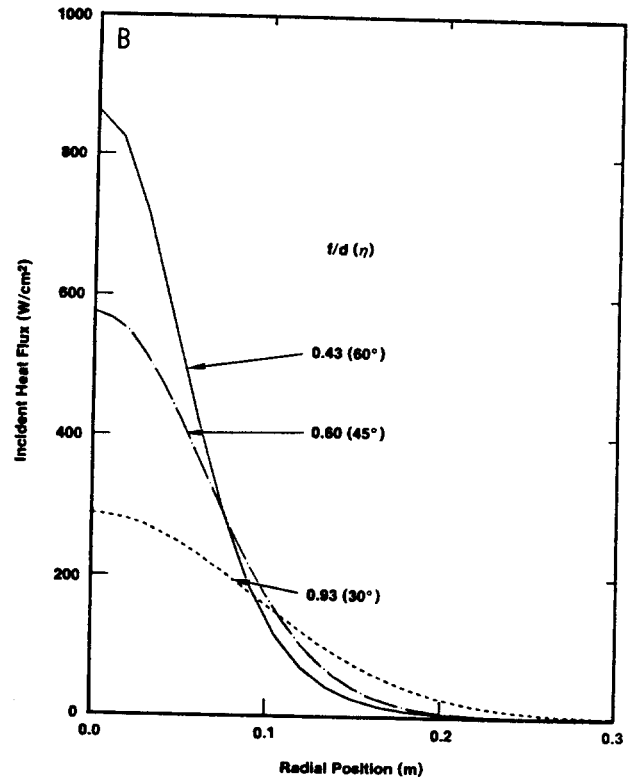
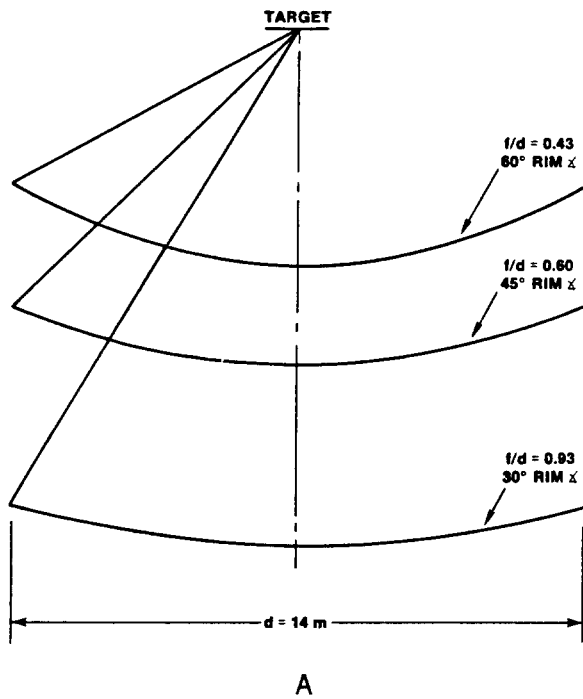


Figure 9: Comparative results for 3 parabolic dishes ($f/d=0.43, 0.6, 0.93$). Figure (a) shows the different curvatures, (b) gives the incident heat flux, and (c) presents the collector optical efficiency as a function of radial position in the focal plane.

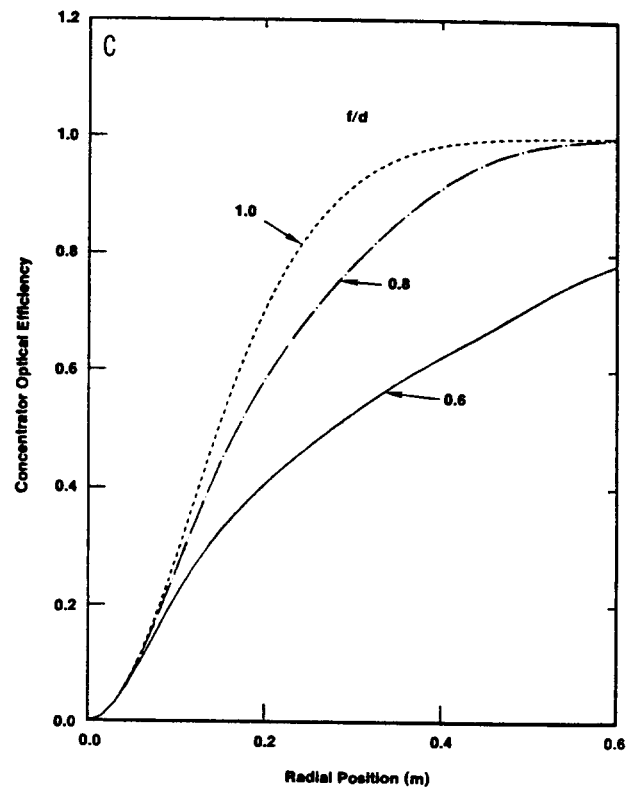
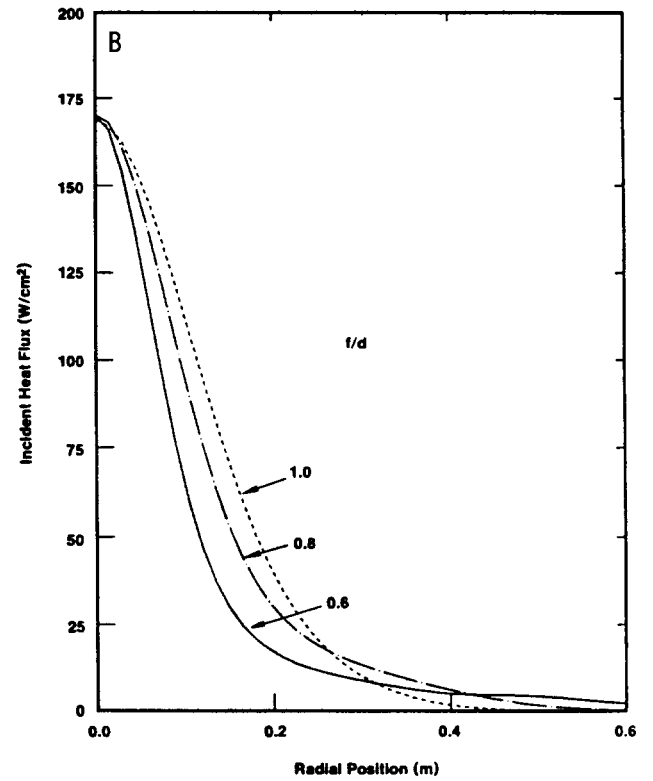
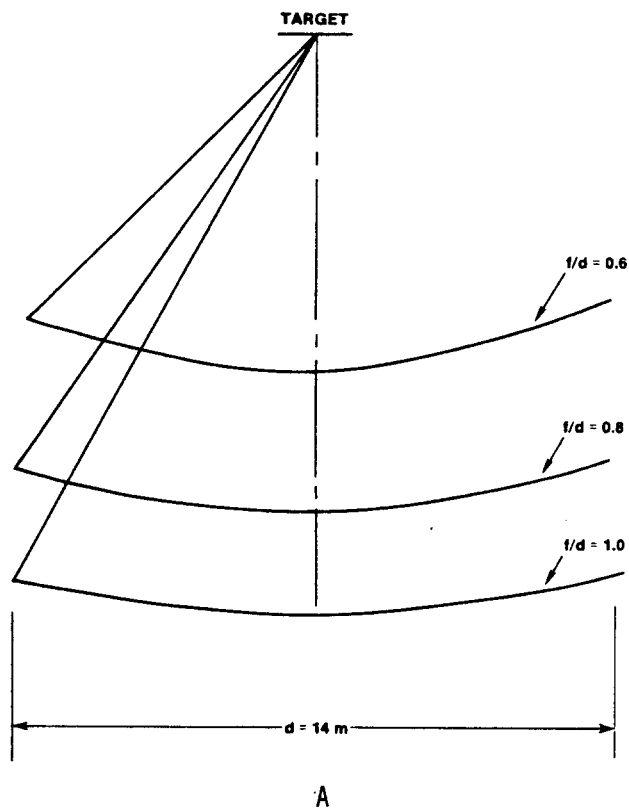


Figure 10: Comparative results for 3 spherical dishes ($f/d=0.6, 0.8, 1.0$). Figure (a) shows the different curvatures, (b) gives the incident heat flux, and (c) presents the collector optical efficiency as a function of radial position in the focal plane.

The results from the spherical dishes are somewhat different from those shown for parabolic dishes. The peak incident heat fluxes are comparable for the three spherical dishes, and are also lower than for the parabolic reflectors. The incident heat flux falls off rapidly with decreasing f/d , as in the parabolic dish comparisons. However, unlike the parabolic dish results, the flux remains nonzero for large radial distances. This would be expected for spherical dishes since the solar flux is reflected to a focal zone rather than to a focal point. The smaller the f/d ratio, the larger the focal zone becomes.

6.2 Example 2: One Vs. Three Facet Reflector Performances

An interesting alternative to the single continuous reflector is the use of an array of smaller reflectors. In theory, the manufacturing and assembly processes could be simplified, and further, reflector slope errors might be smaller. In this example, we compare the performance of a three dish facet system to that of a single dish reflector. The three facets are arranged as shown in Figure 11, such that the centers of each dish are positioned as if they were on the surface of a 45° rim angle parabolic dish 14 m in diameter. The three facets have radii of 4.04 m, and for this example, are assumed to be aimed at the focal point of the equivalent single 14 m dish, *i.e.*, 8.45 m above the dish vertex. The equivalent f/d for each of the smaller dishes is 1.125 and for the single dish $f/d = 0.6$. The total projected area for the 3 aligned facets is equivalent to the single dish, nominally 154 m². Spherical and parabolic contours are considered for the single large dish and the three small dishes.

Optical efficiency results for the four reflector assemblies are given in Figure 12. The results for the single parabolic and spherical reflectors bracket the results for the three dish facet configurations¹⁷. The single parabolic dish reflector is shown to perform best, while the 3 spherical and parabolic dishes perform similarly. The fact that the 3 dishes do not perform as well as the single parabolic dish is not surprising. Each of the facets has a longer focal length than the single paraboloid. More importantly, each of the smaller dishes is canted, so that the incident solar flux is not normal to the projected facet area. Thus, the facets experience astigmatism, *i.e.*, only reflected solar flux from the facet center is directed towards the target aim point. This is shown schematically in Figure 13. To capture the solar flux with the 3 facets aligned off-axis (canted), then, the target must be enlarged, as is indicated in Figure 12.

Figure 14 gives the incident flux profiles for one parabolic dish and for the set of three small parabolic dishes. For the single dish, circumferential symmetry is apparent, while three symmetric “tails” can be seen in the flux profile on the target for the 3 dish reflector. As would be expected, the flux levels are reduced for the three dish reflector, and the incident energy is “smeared” over a larger surface area. Similar trends were seen for the spherical dish cases.

¹⁷Results for the single parabolic and spherical dishes are identical to those presented in the previous section. Note that from Figure 12, it is apparent that the f/d for spherical dishes needs to be greater than 0.6 for the dish to be an effective reflector.

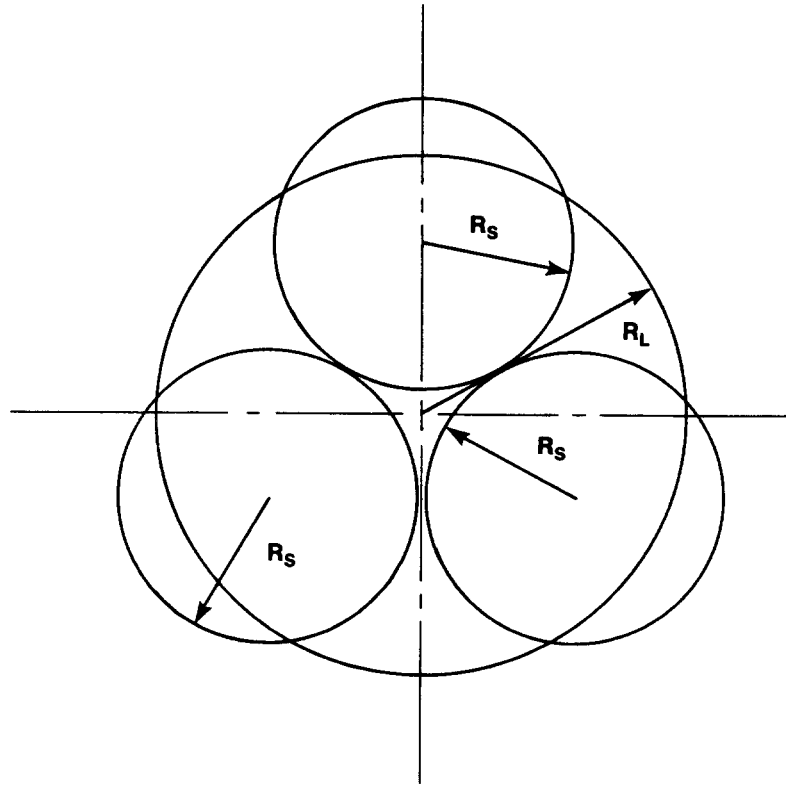


Figure 11: Projected view of single dish and 3 facet reflector systems modeled by CIRCE.

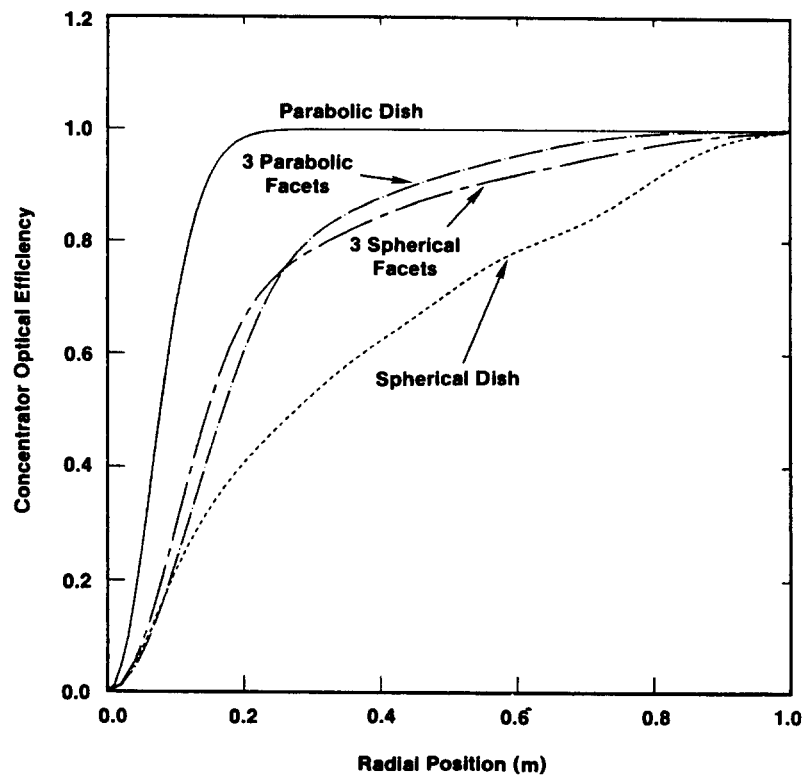


Figure 12: Collector optical efficiency for single dish and 3 facet reflector systems as a function of aperture radius in the focal plane.

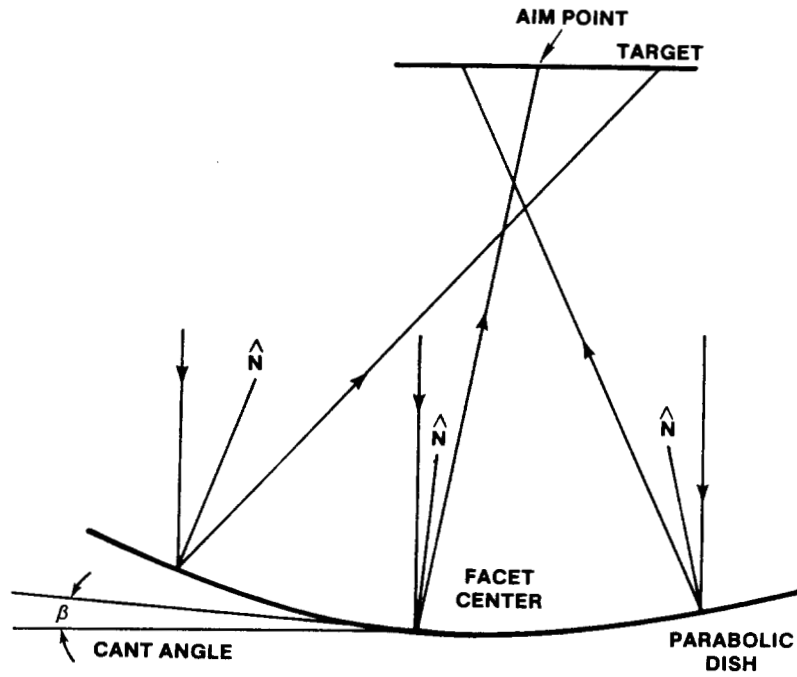


Figure 13: Schematic of canting effects on performance of parabolic dishes.

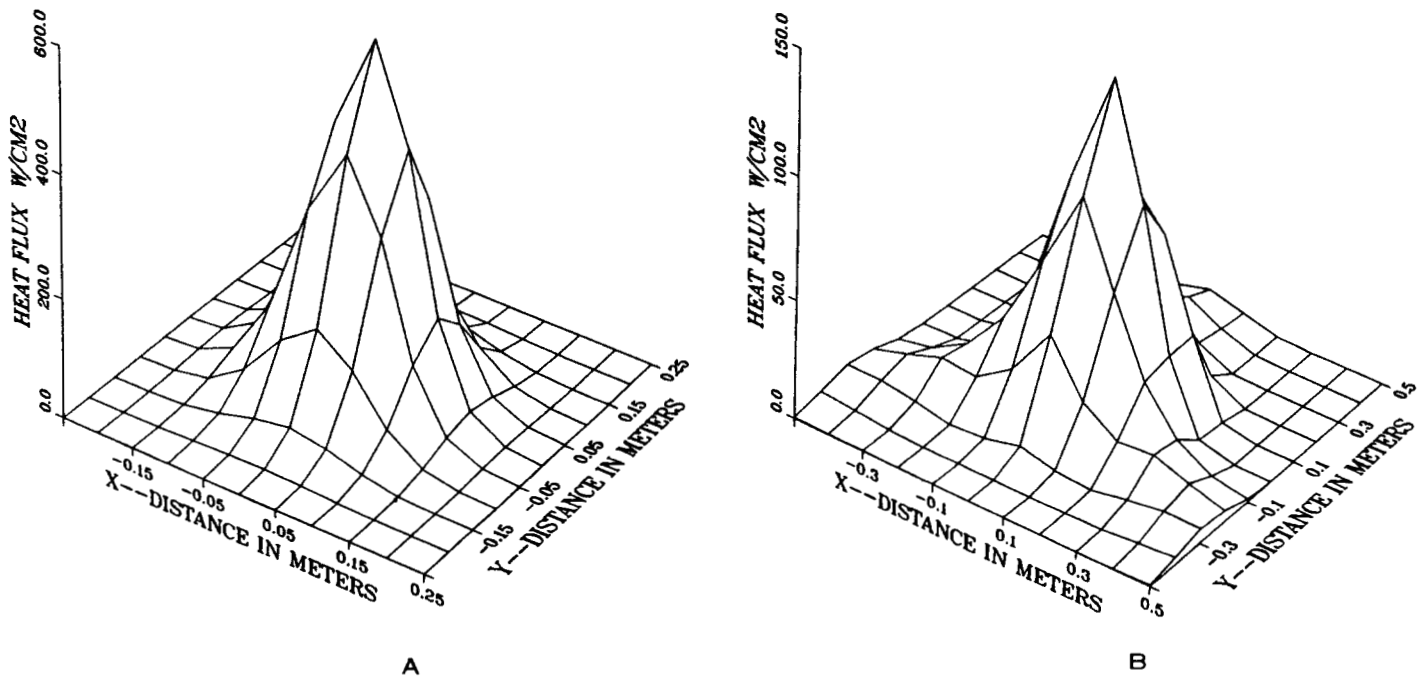


Figure 14: Incident flux profiles on targets from a single parabolic dish (a) and from the 3 parabolic facet reflector system (b).

6.3 Example 3: Test Bed Concentrator #1

An important capability of **CIRCE** is that it can be used to model faceted reflector systems. At present, the authors are unaware of any other existing dish optics simulation which can model both faceted and continuous-surfaced reflectors. Modeling of faceted reflectors is particularly important, given that many of the innovative reflectors that are now being constructed cannot be modeled as continuous surfaces. Notable examples include the LaJet LEC460 [4] (see Figure 1) used at the Solarplant 1 in California and the Power Kinetics Inc., slat reflector used at the Molokai, Hawaii Small Community Solar Experiment #2.

In this example, we have modeled a faceted reflector system referred to as Test Bed Concentrator #1 (TBC-1), installed at the SNLA Solar Thermal Test Facility (STTF). A photograph of TBC-1 is provided in Figure 15. The reflector consists of 220 rectangular facets with spherical contours, each having a projected surface area of 0.438 m^2 . The facets, depending upon location, have different radii of curvature ($\mathcal{R} = 13.2 \text{ m}$, 15.8 m , and 16.1 m); the baseline design configuration is shown schematically in Figure 16. All facets are nominally aimed at a position 7.1 m above the reflector base.

Figure 17 provides incident heat flux on a circular target and also the collector optical efficiency for three different cases. Results for the baseline design are shown as well as results for two off-design configurations. For one of the off-design cases, the radii of curvature for the innermost facets were set to 10.0 m rather than 13.2 m . For the other case, three aim points were considered. For the innermost facets (with $\mathcal{R} = 13.2 \text{ m}$), the aim point was specified as 7.0 m above the reflector vertex, while for the middle facets, the aim point (facets with $\mathcal{R} = 15.8 \text{ m}$) was set to 7.25 m . The aim point for the remaining facets (with $\mathcal{R} = 16.1 \text{ m}$) was maintained at the nominal position of 7.1 m above the vertex.

The performance of the TBC-1 reflector is clearly degraded by altering the aim point locations and the radii of curvature of the innermost facets. Altering the aim points, in particular, results in “smeared” target flux distributions. Additionally, some of the reflected energy completely misses the target for both off-design cases. This is apparent from the optical efficiency curves which asymptote at 0.97 instead of 1.0 . Our calculations indicate that the baseline configuration of the TBC-1 reflector results in nearly optimal performance for this reflector. As evidence of this, calculations were performed modeling the TBC-1 reflector as a continuous 42° rim angle parabolic dish of diameter 10.8 m and using the same effective sunshape given in Figure 8. Results from this model were indistinguishable from the plotted results shown in Figures 17 for the baseline design.



Figure 15: Photograph of Test Bed Concentrator #1 at SNLA.

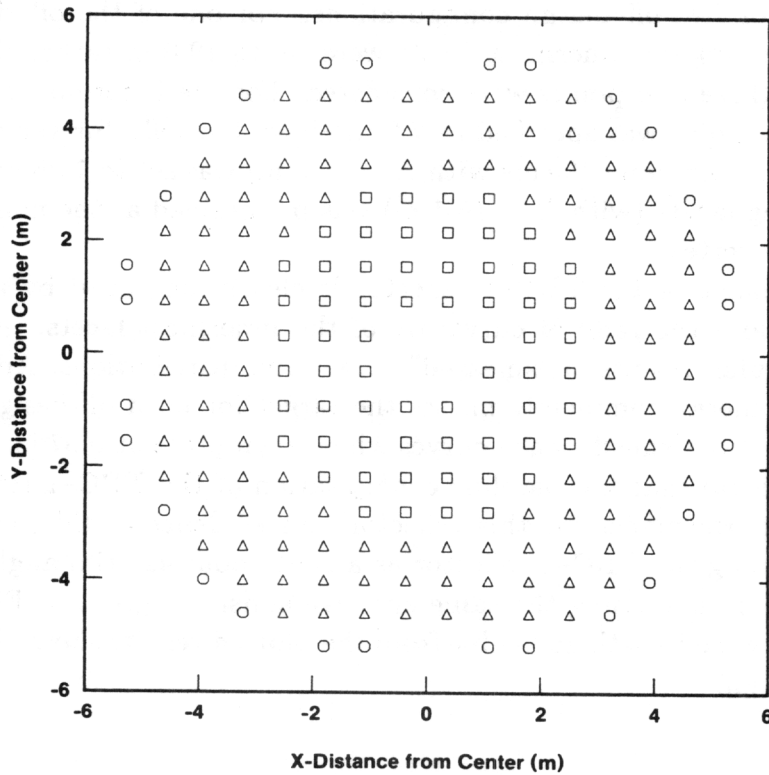


Figure 16: Center positions of 220 facets comprising TBC-1. Square symbols are for facets with radii of curvature $\mathcal{R} = 13.2$ m, triangles for facets with $\mathcal{R} = 15.8$ m, and circles for facets with $\mathcal{R} = 16.1$ m.

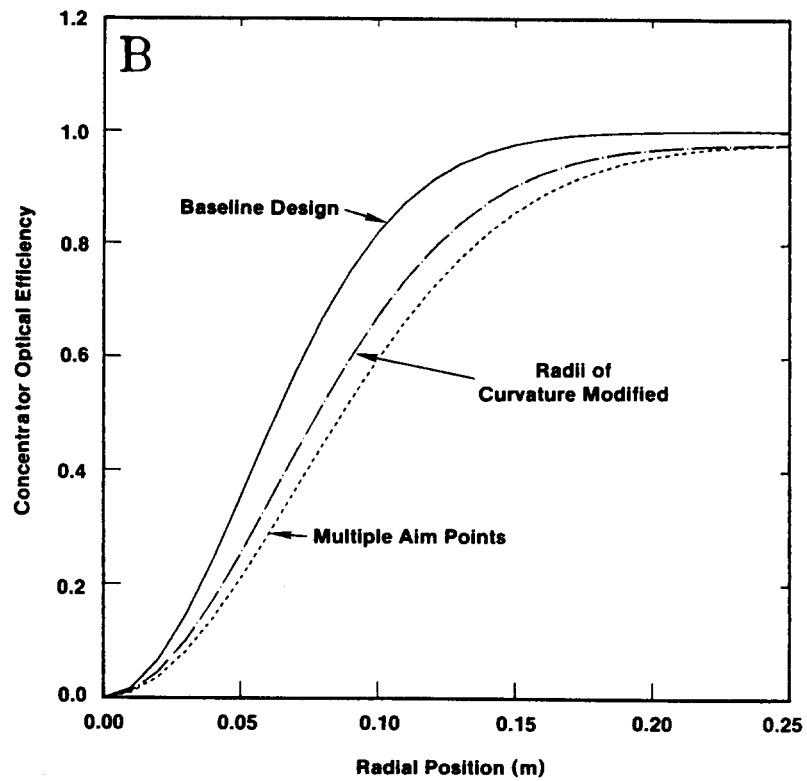
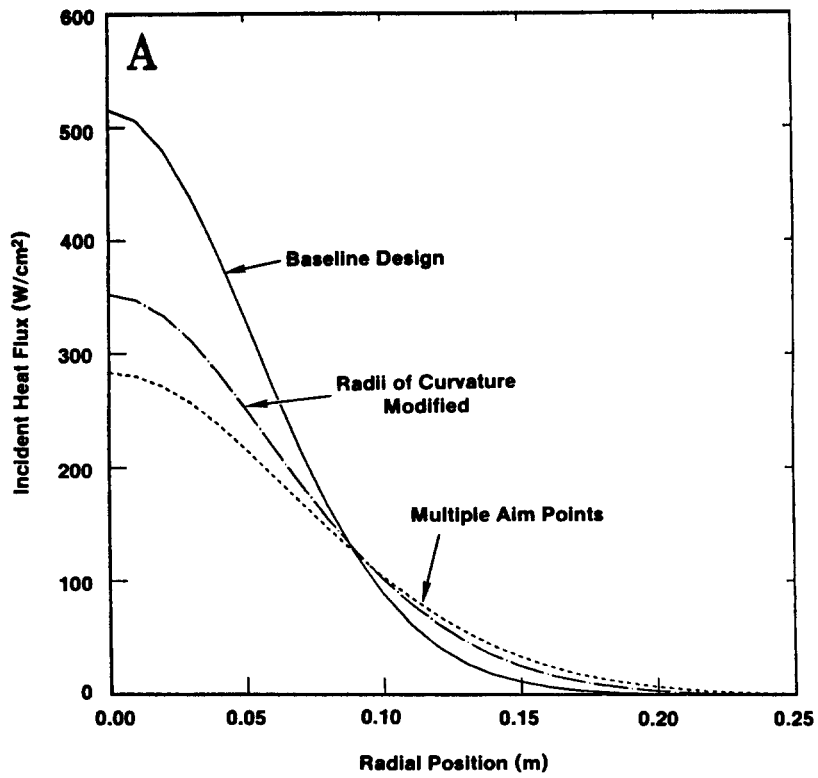


Figure 17: Incident heat flux (a) and collector optical efficiency (b) for the TBC-1 reflector system.

7 CIRCE Usage

Versions of **CIRCE** now exist that execute on VAX computer systems and on personal computers (Additionally, the VAX version of **CIRCE** has been executed on the SNLA CRAY computer during code benchmarking studies.). The implementation of all **CIRCE** options on the PC has not been completed to-date. In particular, a graphics simulation to produce plots of **CIRCE** output has not been completed; this work is in progress. The PC version can currently be used to model concentrator systems with 50 facets or less. We expect that further modifications will result in subsequent versions being able to accommodate solar collector systems comprised of more facets.

In the following subsections, implementation of the **CIRCE** simulation is described for VAX and personal computer systems. A schematic of the execution sequence is provided in Figure 18. Here it is shown that, except for plotting capabilities, the execution steps for **CIRCE** on VAX computer systems and on PCs are comparable. Note that although implementation of **CIRCE** on both VAX and PC systems can be expected to change as additional options are incorporated, we will attempt to maintain analogous structure for these executions.

7.1 Implementation on VAX Computer Systems

The computer codes comprising the **CIRCE** simulation were developed for use on a Digital Equipment Corporation VAX 11/785 computer system using the VMS operating system. Execution of the **CIRCE** simulation on VAX computer systems is performed using the interactive command procedure **CIRCE.COM**. **CIRCE.COM** prompts the user to determine whether plotting or data generation is required as well as for definition of file names, output devices, *etc.*, during execution. It also performs all file manipulations, including file storages, retrievals, and deletions, and also accesses the executable versions of **CIRCE.001**, **DEKGEN**, and **PLOT** from the SNLA Directorate 1500 VAX cluster using DECNET. **CIRCE.COM** has been configured in this manner so that the user will always be able to access the most recent version of the codes saved on the VAX¹⁸. For SNLA VAX users on DECNET, **CIRCE.COM** can be obtained using the following command:

```
COPY SAV03::U2:[ACRATZE.SOLAR]CIRCE.COM CIRCE.COM
```

CIRCE.COM is then executed using the command: **@CIRCE**

¹⁸We request that this policy be followed, *i.e.*, that only the executables should be accessed during the development of the **CIRCE** optics package. The source listings of the simulations are available from the authors, if needed. We have “protected” the Fortran source listings so that the simulations cannot be copied or edited. Upon completion of the previously mentioned updates to **CIRCE**, these restrictions will be relaxed.

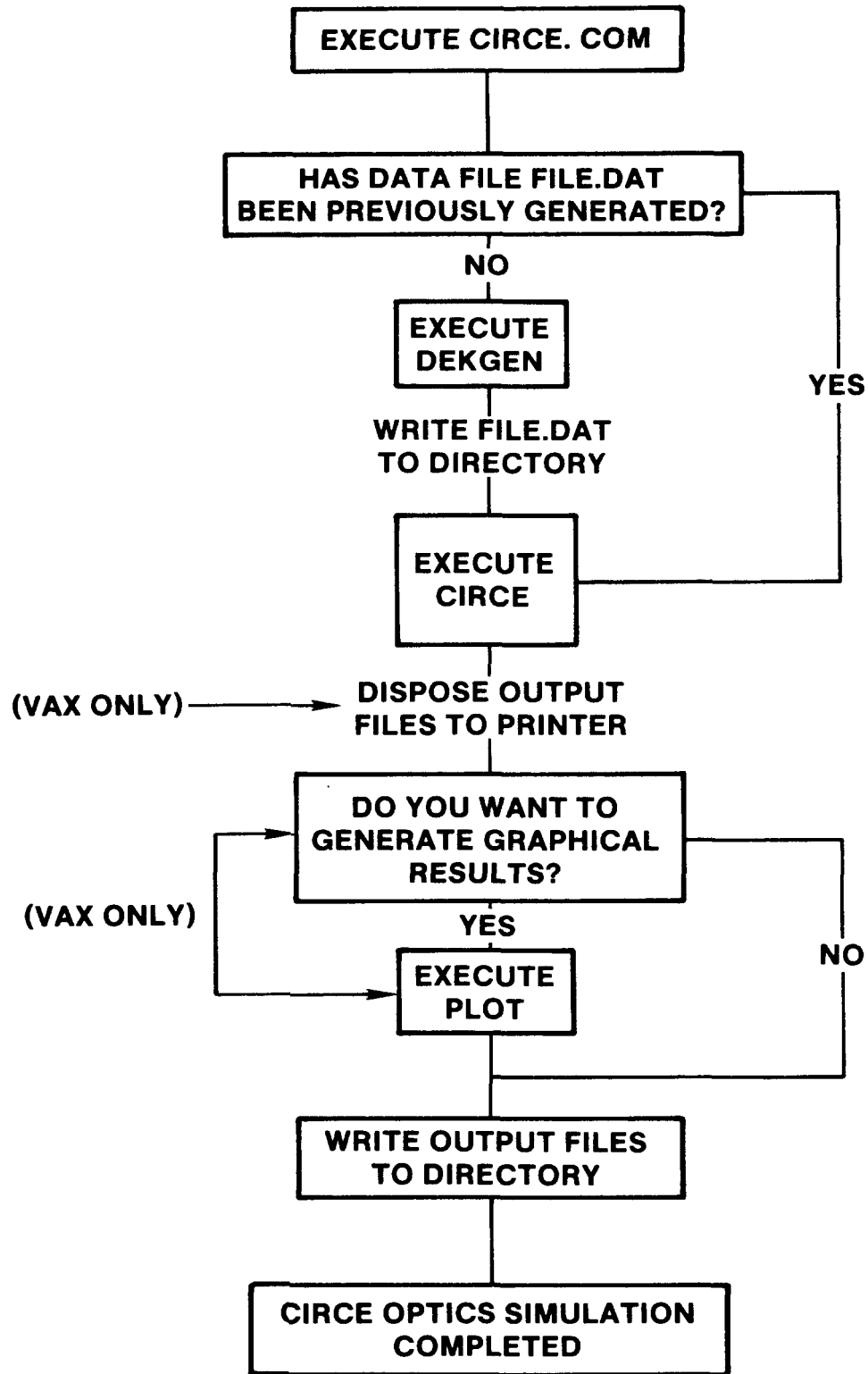


Figure 18: Execution sequence of *CIRCE* simulation on personal computer and VAX computer systems.

The VAX VMS operating system uses a tree-structured file storage system that allows the user to logically group files in different directories. In **CIRCE.COM**, we have built in the capability to utilize this structure. **CIRCE.COM** prompts the user for the directory containing the data file, if previously generated, or for a disposal directory, if a new data file is generated using **DEKGEN**, and also for a disposal directory for output generated by **CIRCE.001** and **PLOT**. While a single directory will suffice for **CIRCE** execution, we recommend using three separate directories for data (**DATA**), for results (**RESULTS**), and for executing **CIRCE.COM** (**WORK**). Figure 19 shows in schematic the directory structure we have used.

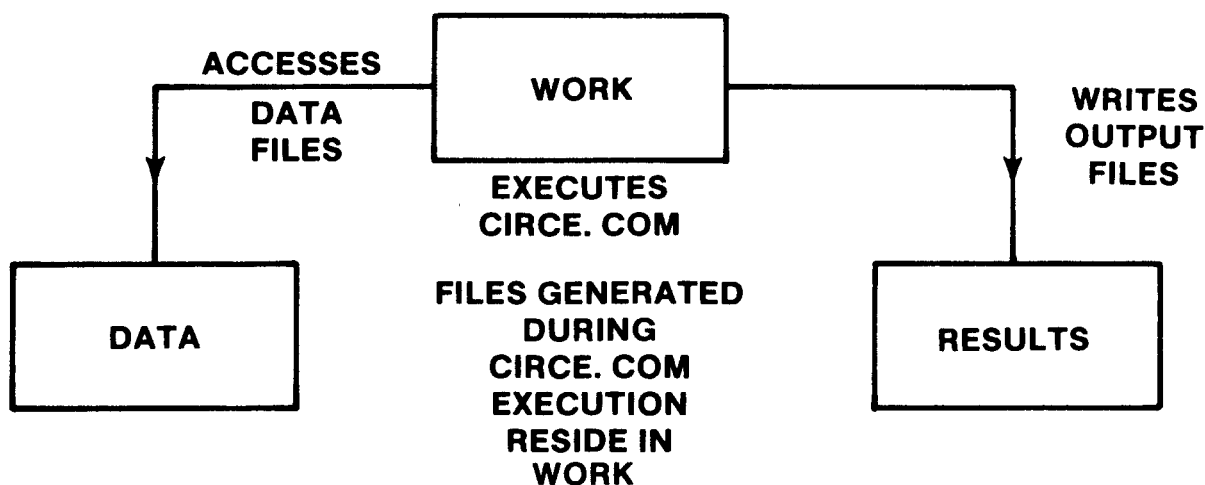


Figure 19: Recommended directory structure for executing **CIRCE** simulation.

WORK

The **WORK** subdirectory serves as the site from which the **CIRCE** simulation is executed; here, the **CIRCE.COM** command procedure should be stored. During execution, scratch files and executables of **CIRCE.001**, **DEKGEN** and **PLOT** reside in **WORK**. Following execution of the simulations, **CIRCE.COM** performs a “clean-up” of **WORK**, transferring results to appropriate locations and deleting unneeded files. In the event of a user abort during execution, this clean-up procedure should delete all executables (see footnote 18), although some intermediate results files will remain. We have intentionally set up the procedure file in this manner so that the user can terminate at any time without losing intermediate files that he may want to review.

RESULTS

Output files are written to subdirectory **RESULTS**. These files include **FILE.OUT**, **FILE.FLX**, and **FILE.PLT**, where “FILE” is the user-specified results file designator. **CIRCE.COM** performs internal “clean-up” of the **RESULTS** directory, eliminating previously obtained output files with the same designator “FILE”; the user should be careful when naming results files to protect previously generated files.

DATA

Data files generated using **DEKGEN** are written to directory **DATA**. Multiple data sets with the same user-specified designator “FILE” are possible in **DATA**, since **CIRCE.COM**, does not delete previously generated **FILE.DAT** files. Additionally, data files that can be accessed during **DEKGEN** execution can be stored in **DATA**. Such files might include, for example, tabulated sunshapes or facet coordinate data.

The **DATA** subdirectory is the least needed of the subdirectories. We recommend that if **DATA** is eliminated, the data files created using **DEKGEN** be written to the **RESULTS** subdirectory along with files such as tabulated sunshapes and reflector geometry data. This would be consistent with the directory structure and philosophy developed for PC execution, discussed in the next section.

7.2 Implementation on Personal Computer Systems

Executable versions of the simulations **DEKGEN** and **CIRCE.001** and the command procedure file **CIRCE.BAT** are available from the authors on floppy disks. This software requires an IBM PC compatible with 640 Kb of RAM, a hard disk, a 8087 math coprocessor and MS-DOS 3.0 or later. As indicated in the introduction of this section, the PC version of **CIRCE** can be used to model reflectors comprised of 50 or less facets. Appropriate prompts in **DEKGEN** will instruct the user as to other limitations imposed when using the PC to execute **CIRCE**. Additionally, there is no software presently available for generating graphical output of **CIRCE** results on the PC. The plot file **FILE.FLX** is, nonetheless, still generated, and the user can employ his own software for presenting the summary results, if desired.

The distribution floppy disks contain an automated installation procedure named **INSTALL.BAT** in the root directory that requires minimal knowledge of MS-DOS. Simply placing the first floppy disk into drive A: and typing **A:INSTALL**, starts the procedure that builds the directory structure and copies all the needed files¹⁹. Additionally, the installation procedure will link the compiled version of **CIRCE.001**.²⁰ An

¹⁹The procedure **INSTALL.BAT** facilitates PC execution of **CIRCE**. An additional command procedure **DEINSTALL.BAT** is also provided in the root directory of floppy disk #1. This procedure will eliminate the files and directories created by **INSTALL**. To implement this procedure, place the floppy into drive A and type **A:DEINSTALL**.

²⁰**CIRCE.001** has been broken into sections **CIRCE** and **MATHC** to facilitate compilation on the PC. These parts are automatically linked by **INSTALL.BAT**.

executable version of **DEKGEN** is provided on the floppy disk. Given the current size of **CIRCE**, an executable version of **CIRCE** could not be transported on floppy disks.

Two directories are created by **INSTALL.BAT**: `\CIRCE` and `\CIRCE\WORK`. Execution of the **CIRCE** simulation occurs within `\CIRCE`, and data and results files are maintained within this directory. The subdirectory `\CIRCE\WORK` contains the object and executable versions of the codes, as well as subsidiary files needed for file linkages. There should be no need for the user to access this subdirectory; all accessing is performed internally by **CIRCE.BAT**.

The **CIRCE** simulation is executed on the PC using **CIRCE.BAT**, which is comparable to **CIRCE.COM** developed for VAX execution (see previous section). **CIRCE.BAT** is an interactive command procedure that performs all file manipulations, including file storages, retrievals, and deletions. Execution of the **CIRCE.BAT** procedure must take place from within the `\CIRCE` directory which is entered by typing `CD \CIRCE` at the `C>` prompt. Once in the `\CIRCE` directory, execution of **CIRCE.BAT** is as simple as typing `CIRCE FILNAM`. Here, `FILNAM` is the name which will be assigned to files (*e.g.*, **FILNAM.DAT**, **FILNAM.OUT**, and **FILNAM.FLX**) that will be created during execution of **CIRCE** and **DEKGEN**.

The command procedure file **CIRCE.BAT** is configured to execute the **CIRCE** simulation on the PC in the same manner that **CIRCE.COM** executes the simulation on VAX computers. Execution of the input deck generator **DEKGEN** can be bypassed if the user inputs the name of an already existing data file `FILENAM`²¹. Otherwise, the input file can be created by the user answering the interactive prompts, or the user can edit an existing data file. Next, **CIRCE.001** is executed. Execution times will be longer than for PCs for VAX systems, but the numerical accuracy of the results should be comparable. The user should limit the number of facet and target subdivisions, where possible, during parameter studies. If more refined results are needed, these parameters can be increased at the expense of execution time.

7.3 Execution Time Comparisons

Results presented in this report were obtained using VAX 11/785 and VAX/8650 computers, and also an IBM-XT personal computer. Although the simulation is intended for much smaller systems, **CIRCE** has also been run, during benchmark studies, on a CRAY computer system. Results obtained from the different systems are comparable within $\pm 1.0\%$, suggesting that there is little loss in accuracy when smaller systems are used. **CIRCE** execution times do vary considerably, however, for the different computer systems. As an example, we present execution times for the single parabolic dish and the 3 facet concentrator system analyzed in Example 2.

²¹Users should be careful to rename data files before executing **CIRCE** on PCs, particularly if previously output files were generated using the same name, since output files having the same name will be overwritten. The command procedure will indicate that output files were previously generated with the same name, and the user can abort **CIRCE.BAT** execution rather than overwriting the results files.

Table 4: **CIRCE** Execution Times in Seconds for Example 2

Case Analyzed	IBM PC-XT	VAX/785	VAX/8650
Single Parabolic Dish	406	7.8	0.24
3 Facet Concentrator	2640	41.1	2.1

It should be noted that the execution time increases as a function of the number of target points multiplied by the total number of subfacets. For multi-faceted reflector systems, it is recommended that the user minimize the number of subfacet divisions for initial executions on personal computers.

8 Example Data Files and Output

Listings of two data files are provided in Appendix B. One (designated **45DEG.DAT**) is for the 14-m diameter 45° rim angle parabolic dish of Example 1 (Section 6.1) and the second (designated **3PDISH.DAT**) is for the three parabolic facet concentrator example presented in Section 6.2.

The example data files are included on PC floppy disk #1, to be provided from the authors upon request. For VAX users on DECNET, these files can be accessed using the following command:

```
COPY SAV03::U2:[ACRATZE.SOLAR]data.fil data.fil
```

where *data.fil* is either file **45DEG.DAT** or **3PDISH.DAT**.

We recommend that novice users of **CIRCE** execute **CIRCE** using these data files. The user can also use these files when creating files with **DEKGEN**. Parts of the output generated for each example (executing **CIRCE** on the SNLA Directorate 1500 11/785 VAX computer) are also provided in Appendix B, for comparison. This output, and the graphical results presented in Section 6, should allow the user to benchmark his results with the presented results.

9 References

1. C. C. Wan, "CAV" Code for the Determination of Incident Flux Distribution in an Axisymmetrical Cavity from a Paraboloidal Reflector, Ford Aerospace & Communications Corp. Technical Report SCSE-016, July, 1980.
2. *Concentrator Optical Performance Software (COPS) User's Manual*, Honeywell Inc. Report DOE/CS/35348-T1 (Vol.2), January, 1980.
3. F. Biggs and C. N. Vittitoe, *The Helios Model for the Optical Behavior of Reflecting Solar Concentrators*, Sandia National Laboratories Report SAND76-0347, March, 1979.
4. D. Carroll, *SOLARPLANT1*, Sun World, Vol.9, No.1, 1985.
5. G. S. Kinoshita, *The Shenandoah Parabolic Dish Solar Collector*, Sandia National Laboratories Report SAND83-0583, January, 1985.
6. G. L. Schrenk and D. G. Gritton, *Analysis of Solar Reflectors - Mathematical Theory and Methodology for Simulation of Real Reflectors*, GMC-AO-EDR3693, December, 1963.
7. C. N. Vittitoe and F. Biggs, *A User's Guide to Helios: A Computer Program for Modeling the Optical Behavior of Reflecting Solar Concentrators, Part I. Introduction and Code Input*, Sandia National Laboratories Report SAND81-1180, August, 1981.
8. C. N. Vittitoe and F. Biggs, *A User's Guide to Helios: A Computer Program for Modeling the Optical Behavior of Reflecting Solar Concentrators, Part III. Appendices Concerning Helios - Code Details*, Sandia National Laboratories Report SAND81-1562, September, 1981.
9. *DISSPLA User's Manual*, developed by Integrated Software Systems Corporation, 1978.
10. V. R. Goldberg, *Test Bed Concentrator (TBC)*, Proceedings of the First Semianual Distributed Receiver Systems Program Review, January 22-24, 1980, Lubbock, Texas, DOE/JPL-1060-33, April, 1980.
11. R. B. Diver, ed., *Proceedings of the Solar Thermal Technology Conference, Albuquerque, NM, June 17-19, 1986*, Sandia National Laboratories Report SAND86-0536, June, 1986.

Appendix A

A Variables Used in DEKGEN

General Problem Parameters

<u>Variable</u>	<u>Description</u>	<u>Units</u>
IPLOT	Identifier for plot file generation option	
IPRINT	Identifier for print options	
PHIL	Reflector latitude	[degrees]
SDAY	Day of analysis	[day]
SOLTIM	Time of day	[hours]
TITLE	General problem parameters title descriptor	

Sun and Error Parameters

<u>Variable</u>	<u>Description</u>	<u>Units</u>
ALO	Start of sun limb	[milliradians]
BLIM	End of sun limb	[milliradians]
IANLYT	Identifier for convolution of errors and sunshape	
IDL	Limb darkening identifier	
IDIM	Identifier for dimensionality of effective sunshape	
JSUN	Sunshape type	
NER	Number of reflector errors	
NTR	Tracking error option	
NTABL	Number of values for tabular sunshape	
RHO	Sun angle with respect to sun central ray	[degrees]
SI	Solar flux intensity	[W/m ²]
SIGX	Major axis standard deviation of elliptic normal error distribution	[milliradians]
SIGY	Minor axis standard deviation of elliptic normal error distribution	[milliradians]
SVAL	Tabulated sunshape magnitude	
SUNTIT	Sun and error parameters descriptor	
TH	Rotation angle for elliptic normal error distribution	[milliradians]
TRH	Horizontal elevation tracking error	[milliradians]
TRV	Vertical azimuthal tracking error	[milliradians]

Target/Receiver Parameters

<u>Variable</u>	<u>Description</u>	<u>Units</u>
DRAD	Parabolic dish radius	[m]
DXTARGI	X position on target (I=1,3)	[m]
DYTARGI	Y position on target (I=1,3)	[m]
DZTARGI	Z position on target (I=1,3)	[m]
IAPT	Cavity receiver identifier (option not used in CIRCE.001)	
IRECP	Reconcentrator identifier (option not used in CIRCE.001)	
ISHAD	Target blockage identifier	
ITARSH	Target shape identifier	
IXPTS	Number of subdivisions in x directions of rectangular or number of radial subdivisions for circular target	
IYPTS	Number of subdivisions in y directions of rectangular or number of circumferential subdivisions for circular target	
NFLSV	Target position identifiers for facet flux printout	
NFOC	Number of target aim points	
NTAGP	Target position identifier for printout of D_{ij}	
NTARSV	Number of target positions for facet flux printout	
RIMANG	Parabolic dish rim angle	[degrees]
SHADR	Target blockage radius	[m]
TARTIT	Target/receiver target parameters title descriptor	
XEXT	X extent of rectangular or radius of circular target	[m]
YEXT	Y extent of rectangular target	[m]

Reflector/Facet Parameters

<u>Variable</u>	<u>Description</u>	<u>Units</u>
ASUB	Coefficients of the polynomial series for IOPT=4	
ELENX	X extent of rectangular facet	[m]
ELENY	Y extent of rectangular facet	[m]
FLENG	Radius of circular facet	[m]
FOCL	Focal length of parabolic facet	[m]
FOC	Focal length of parabolic facet or radius of curvature for spherical facet	[m]
KORD	Identifier for projected shape of facet	
ICPQR	Identifier for input of facet normals	
IDF	Identifier for facet	
IOPT	Identifier for facet contour	
ITERM	Number of terms for the polynomial series for IOPT=4	
NFACET	Number of facets comprising the reflector	
NFID	Aim point identifier for facet	
NSUBF	Number of radial subdivisions for circular facet	
NX	Number of subdivisions in x direction for rectangular facet	
NY	Number of subdivisions in y direction for rectangular facet	
PN,QN,RN	X,Y,Z components of facet normal	
RCURV	Radius of curvature of spherical facet	[m]
REFLEC	Solar specular reflectivity of facet	
REFTIT	Reflector/facet parameters title descriptor	
SBM	Blockage factor for facet	
U1,U2,U3	X,Y,Z coordinates of facet center	[m]

Appendix B

B Example Data Files and Results

B.1 Example 1: 45° Rim Angle Parabolic Dish

The data file and some of the output generated for the 14-m 45° rim angle parabolic dish geometry presented in Example 1 (Section 6.1) are provided here. We have included the variable names (in parentheses) in the data set to facilitate the user's duplication of this file when executing **DEKGEN**. The output was generated using a VAX 11/785 computer.

B.1.1 45DEG.DAT File

7M RADIUS 45DEG PARABOLIC DISH	
0 1 0.000 80.000 34.960	(TITLE)
TABULAR SUN - 1-D NUMERICAL CONVOLUTION	(IPRINT, IPLOT, SOLTIM, SDAY, PHIL)
1 .10000	(SUNTIT)
18	(JSUN, S)
.00000E+00 202.40	(NTABL)
.22000E-03 202.40	(RHO(I), SVAL(I), I=1, NTABL)
.65000E-03 202.40	"
.10900E-02 200.28	"
.15300E-02 197.10	"
.19600E-02 192.86	"
.24000E-02 188.63	"
.28400E-02 182.27	"
.32700E-02 172.73	"
.37100E-02 155.78	"
.41500E-02 105.97	"
.45800E-02 7.5030	"
.50200E-02 .28300	"
.54501E-02 .17600	"
.58901E-02 .12100	"
.63301E-02 .88000E-01	"
.67601E-02 .74000E-01	"
.72001E-02 .66000E-01	"
2 1 1 0	(NER, NTR, IDIM, IANLYT)
.00000E+00 .25000E-02 .25000E-02	(TH(1), SIGX(1), SIGY(1))
.00000E+00 .15000E-02 .15000E-02	(TH(2), SIGX(2), SIGY(2))
.12000E-02 .12000E-02	(TRH, TRV)
.5M RADIUS CIRCULAR TARGET — NO BLOCKAGE	(TARTIT)
0 6 0 0	(IAPT, ITARSH, IRECP, ISHAD)
.5000 6.283 51 1	(XEXT, YEXT, IXPTS, IYPTS)
0.000000E+00 -4.809025E+00 6.947713E+00	(XTARG(1), YTARG(1), ZTARG(1))
-2.500000E-01 -4.809025E+00 6.947713E+00	(XTARG(2), YTARG(2), ZTARG(2))
0.000000E+00 -2.225870E+00 8.735705E+00	(XTARG(3), YTARG(3), ZTARG(3))
1	(NFOC)
1 0.000000E+00 -4.809025E+00 6.947713E+00	(I, XFOC, YFOC, ZFOC)
7M RADIUS PARABOLIC DISH — 10 RADIAL SUB	(TARTIT)
1 1 1 0 1.000	(NFACET, KORD, IOPT, ICPQR, REFLEC)
7.0000 10	(FLENG, NSUBF)
1 0.0000 0.0000 0.0000 8.4497 0.000 1	(IDF, U1, U2, U3, FOC, SBM, NFID)

B.1.2 Partial Results from 45DEG.OUT

```
***** FLUX DISTRIBUTION ON TARGET (W/CM2) *****
R(I)  THETA=  0.0000
 0.0000  5.761E+02
 0.0100  5.665E+02
 0.0200  5.486E+02
 0.0300  5.144E+02
 0.0400  4.729E+02
 0.0500  4.238E+02
 0.0600  3.709E+02
 0.0700  3.171E+02
 0.0800  2.650E+02
 0.0900  2.167E+02
 0.1000  1.731E+02
 0.1100  1.357E+02
 0.1200  1.042E+02
 0.1300  7.838E+01
 0.1400  5.808E+01
 0.1500  4.216E+01
 0.1600  3.020E+01
 0.1700  2.131E+01
 0.1800  1.482E+01
 0.1900  1.021E+01
 0.2000  6.927E+00
 0.2100  4.681E+00
 0.2200  3.117E+00
 0.2300  2.061E+00
 0.2400  1.360E+00
 0.2500  8.816E-01
 0.2600  5.750E-01
 0.2700  3.655E-01
 0.2800  2.328E-01
 0.2900  1.469E-01
 0.3000  9.121E-02
 0.3100  5.672E-02
 0.3200  3.498E-02
 0.3300  2.115E-02
 0.3400  1.282E-02
 0.3500  7.650E-03
 0.3600  4.290E-03
 0.3700  2.578E-03
 0.3800  1.428E-03
 0.3900  6.214E-04
 0.4000  3.699E-04
 0.4100  6.001E-05
 0.4200  0.000E+00
 0.4300  0.000E+00
 0.4400  0.000E+00
 0.4500  0.000E+00
 0.4600  0.000E+00
 0.4700  0.000E+00
 0.4800  0.000E+00
 0.4900  0.000E+00
 0.5000  0.000E+00
```

OPTICAL EFFICIENCY FOR DISK APERTURE

RADIUS (M)	EFFICIENCY
0.0000E+00	0.0000E+00
1.0000E-02	1.1641E-02
2.0000E-02	4.5782E-02
3.0000E-02	1.0000E-01
4.0000E-02	1.7047E-01
5.0000E-02	2.5274E-01
6.0000E-02	3.4181E-01
7.0000E-02	4.3289E-01
8.0000E-02	5.2175E-01
9.0000E-02	6.0502E-01
1.0000E-01	6.8027E-01
1.1000E-01	7.4610E-01
1.2000E-01	8.0206E-01
1.3000E-01	8.4830E-01
1.4000E-01	8.8560E-01
1.5000E-01	9.1501E-01
1.6000E-01	9.3767E-01
1.7000E-01	9.5483E-01
1.8000E-01	9.6758E-01
1.9000E-01	9.7692E-01
2.0000E-01	9.8365E-01
2.1000E-01	9.8844E-01
2.2000E-01	9.9181E-01
2.3000E-01	9.9415E-01
2.4000E-01	9.9577E-01
2.5000E-01	9.9687E-01
2.6000E-01	9.9762E-01
2.7000E-01	9.9812E-01
2.8000E-01	9.9845E-01
2.9000E-01	9.9866E-01
3.0000E-01	9.9880E-01
3.1000E-01	9.9889E-01
3.2000E-01	9.9895E-01
3.3000E-01	9.9899E-01
3.4000E-01	9.9901E-01
3.5000E-01	9.9902E-01
3.6000E-01	9.9903E-01
3.7000E-01	9.9904E-01
3.8000E-01	9.9904E-01
3.9000E-01	9.9904E-01
4.0000E-01	9.9904E-01
4.1000E-01	9.9904E-01
4.2000E-01	9.9904E-01
4.3000E-01	9.9904E-01
4.4000E-01	9.9904E-01
4.5000E-01	9.9904E-01
4.6000E-01	9.9904E-01
4.7000E-01	9.9904E-01
4.8000E-01	9.9904E-01
4.9000E-01	9.9904E-01
5.0000E-01	9.9904E-01

*** INTEGRATION FOR FLAT CIRCULAR TARGET ***

INTEGRATED FLUX USING GAUS8 AND QNC7 = 1.5379E+05 WATTS.

**** SUMMARY RESULTS ****

FACET AREA = 153.9 M**2
 REDUCED BY COS GIVES 153.9 M**2
 FURTHER REDUCED BY SHBL GIVES 153.9 M**2
 POWER INTERCEPTED BY MIRRORS = 0.1539E+06 WATTS.
 NO SHBL EFFECTS INCLUDED.
 SOLAR INSOLATION = 0.10000 W/CM**2
 NO. SUNS IN PEAK = 5760.72
 POWER COLLECTED (GAUS8 & QNC7 INTEG) = 0.1538E+06 W
 TARGET OPTICAL EFFICIENCY = 0.9990E+00

B.2 Example 2: 3 Parabolic Facet Concentrator

The data file and some of the output generated for the 3 facet reflector comprised of 8.1-m 45° rim angle parabolic dishes (presented in Example 2, Section 6.2) are provided here. We have included the variable names (in parentheses) in the data set to facilitate the user's duplication of this file when executing DEKGEN. The output was generated using a VAX 11/785 computer.

B.2.1 3PDISH.DAT File

3 PARABOLIC DISHES — F/D = 1.125	(TITLE)
0 1 0.000 80.000 34.960	(IPRINT, I PLOT, SOLTIM, SDAY, PHIL)
1KW TABULAR SUN — 1-D CONVOLUTION	(SUNTIT)
1 .10000	(JSUN, S)
18	(NTABL)
.00000E+00 202.40	(RHO(I), SVAL(I), I=1, NTABL)
.22000E-03 202.40	"
.65000E-03 202.40	"
.10900E-02 200.28	"
.15300E-02 197.10	"
.19600E-02 192.86	"
.24000E-02 188.63	"
.28400E-02 182.27	"
.32700E-02 172.73	"
.37100E-02 155.78	"
.41500E-02 105.97	"
.45800E-02 7.5030	"
.50200E-02 .28300	"
.54501E-02 .17600	"
.58901E-02 .12100	"
.63301E-02 .88000E-01	"
.67601E-02 .74000E-01	"
.72001E-02 .66000E-01	"
2 1 1 0	(NER, NTR, IDIM, IANLYT)
.00000E+00 .25000E-02 .25000E-02	(TH(1), SIGX(1), SIGY(1))
.00000E+00 .15000E-02 .15000E-02	(TH(2), SIGX(2), SIGY(2))
.12000E-02 .12000E-02	(TRH, TRV)
CIRC TARGET AT FOCAL POINT OF 14M 45DEG PAR DISH	(TARTIT)
0 6 0 0	(IAPT, ITARSH, IRECP, ISHAD)
1.0000 6.283 51 11	(XEXT, YEXT, IXPTS, IYPTS)
0.000000E+00 0.000000E+00 8.4497E+00	(XTARG(1), YTARG(1), ZTARG(1))
2.500000E-01 0.000000E+00 8.4497E+00	(XTARG(2), YTARG(2), ZTARG(2))
0.000000E+00 3.141593E+00 8.4497E+00	(XTARG(3), YTARG(3), ZTARG(3))
1	(NFOC)
1 0.000000E+00 0.000000E+00 8.4497E+00	(I, XFOC, YFOC, ZFOC)
3 PARABOLIC DISH FACETS — FOC=9.095M, R=4.040M	(REFTIT)
3 1 1 0 1.000	(NFACET, KORD, IOPT, ICPQR, REFLEC)
4.040 5	(FLENG, NSUBF)
1 4.0410 2.3333 0.6440 9.0950 0.000 1	(IDF, U1, U2, U3, FOC, SBM, NFID)
2 -4.0410 2.3333 0.6440 9.0950 0.000 1	"
3 0.0000 -4.6667 0.6440 9.0950 0.000 1	"

B.2.2 Partial Results from 3PDISH.OUT

R(I) METERS	THETA=	0.6283	1.2566	1.8850	2.5133	3.1416	3.7699	4.3982	5.0265	5.6549	6.2832	RAD
0.0000	1.343E+02											
0.0200	1.318E+02											
0.0400	1.248E+02	1.244E+02	1.251E+02	1.244E+02	1.244E+02	1.248E+02	1.248E+02	1.246E+02	1.246E+02	1.246E+02	1.246E+02	1.246E+02
0.0600	1.144E+02	1.132E+02	1.153E+02	1.153E+02	1.132E+02	1.144E+02	1.144E+02	1.136E+02	1.136E+02	1.136E+02	1.136E+02	1.136E+02
0.0800	1.021E+02	1.037E+02										
0.1000	8.911E+01	8.578E+01	9.168E+01	9.168E+01	8.578E+01	8.911E+01	8.911E+01	8.695E+01	8.695E+01	8.695E+01	8.695E+01	8.695E+01
0.1200	7.659E+01	7.270E+01	8.014E+01	8.014E+01	7.269E+01	7.657E+01	7.657E+01	7.393E+01	7.393E+01	7.393E+01	7.393E+01	7.393E+01
0.1400	6.466E+01	6.113E+01	6.917E+01	6.917E+01	6.112E+01	6.466E+01	6.466E+01	6.194E+01	6.194E+01	6.194E+01	6.194E+01	6.194E+01
0.1600	5.354E+01	5.133E+01	5.866E+01	5.866E+01	5.134E+01	5.354E+01	5.354E+01	5.120E+01	5.120E+01	5.120E+01	5.120E+01	5.120E+01
0.1800	4.295E+01	4.309E+01	4.854E+01	4.854E+01	4.308E+01	4.294E+01	4.294E+01	4.159E+01	4.159E+01	4.159E+01	4.159E+01	4.159E+01
0.2000	3.315E+01	3.626E+01	3.857E+01	3.856E+01	3.625E+01	3.315E+01	3.315E+01	3.306E+01	3.306E+01	3.306E+01	3.306E+01	3.306E+01
0.2200	2.431E+01	3.071E+01	2.907E+01	2.906E+01	3.073E+01	2.432E+01	2.432E+01	2.579E+01	2.579E+01	2.579E+01	2.579E+01	2.579E+01
0.2400	1.684E+01	2.634E+01	2.052E+01	2.634E+01	1.684E+01	1.684E+01	1.684E+01	1.977E+01	1.977E+01	1.977E+01	1.977E+01	1.977E+01
0.2600	1.100E+01	2.303E+01	1.339E+01	2.302E+01	1.101E+01	1.101E+01	1.101E+01	1.512E+01	1.512E+01	1.512E+01	1.512E+01	1.512E+01
0.2800	6.792E+00	2.043E+01	8.036E+00	8.026E+00	2.042E+01	6.792E+00	6.792E+00	1.049E+01	1.049E+01	1.049E+01	1.049E+01	1.049E+01
0.3000	4.004E+00	1.838E+01	4.390E+00	4.388E+00	1.839E+01	4.004E+00	4.004E+00	5.850E+00	5.850E+00	5.850E+00	5.850E+00	5.850E+00
0.3200	2.311E+00	1.669E+01	2.180E+00	2.178E+00	1.669E+01	2.310E+00	2.310E+00	7.302E+00	7.302E+00	7.302E+00	7.302E+00	7.302E+00
0.3400	1.344E+00	1.518E+01	9.805E-01	9.779E-01	1.518E+01	1.343E+00	1.343E+00	5.955E+00	5.955E+00	5.955E+00	5.955E+00	5.955E+00
0.3600	7.969E-01	1.376E+01	4.063E-01	4.058E-01	1.377E+01	7.971E-01	7.971E-01	5.221E-01	5.221E-01	5.221E-01	5.221E-01	5.221E-01
0.3800	5.022E-01	1.246E+01	1.537E-01	1.535E-01	1.247E+01	5.021E-01	5.021E-01	1.883E-01	1.883E-01	1.883E-01	1.883E-01	1.883E-01
0.4000	3.351E-01	1.124E+01	5.378E-02	5.372E-02	1.124E+01	3.352E-01	3.352E-01	6.012E-02	6.012E-02	6.012E-02	6.012E-02	6.012E-02
0.4200	2.317E-01	1.009E+01	1.761E-02	1.760E-02	1.009E+01	2.316E-01	2.316E-01	1.698E-02	1.698E-02	1.698E-02	1.698E-02	1.698E-02
0.4400	1.657E-01	9.099E+00	6.011E-03	6.010E-03	9.106E+00	1.657E-01	1.657E-01	3.988E-03	3.988E-03	3.988E-03	3.988E-03	3.988E-03
0.4600	0.4600	8.222E+00	2.051E-03	2.051E-03	8.225E+00	1.217E-01	1.217E-01	6.297E-04	6.297E-04	6.297E-04	6.297E-04	6.297E-04
0.4800	8.687E-02	7.504E+00	6.506E-04	6.508E-04	7.510E+00	8.682E-02	8.682E-02	0.000E+00	0.000E+00	0.000E+00	0.000E+00	0.000E+00
0.5000	6.339E-02	6.896E+00	3.000E-04	3.011E-04	6.901E+00	6.324E-02	6.324E-02	0.000E+00	0.000E+00	0.000E+00	0.000E+00	0.000E+00
0.5200	4.519E-02	6.421E+00	2.076E-04	2.079E-04	6.426E+00	4.517E-02	4.517E-02	0.000E+00	0.000E+00	0.000E+00	0.000E+00	0.000E+00
0.5400	3.302E-02	6.050E+00	1.398E-04	1.398E-04	6.048E+00	3.297E-02	3.297E-02	0.000E+00	0.000E+00	0.000E+00	0.000E+00	0.000E+00
0.5600	2.197E-02	5.399E+00	0.000E+00	0.000E+00	5.408E+00	1.520E-02	1.520E-02	0.000E+00	0.000E+00	0.000E+00	0.000E+00	0.000E+00
0.5800	1.024E-02	5.113E+00	0.000E+00	0.000E+00	5.113E+00	1.021E-02	1.021E-02	0.000E+00	0.000E+00	0.000E+00	0.000E+00	0.000E+00
0.6000	6.425E-03	4.782E+00	0.000E+00	0.000E+00	4.782E+00	6.418E-03	6.418E-03	0.000E+00	0.000E+00	0.000E+00	0.000E+00	0.000E+00
0.6200	4.114E-03	4.434E+00	0.000E+00	0.000E+00	4.438E+00	4.120E-03	4.120E-03	0.000E+00	0.000E+00	0.000E+00	0.000E+00	0.000E+00
0.6400	2.457E-03	4.042E+00	0.000E+00	0.000E+00	4.047E+00	2.455E-03	2.455E-03	0.000E+00	0.000E+00	0.000E+00	0.000E+00	0.000E+00
0.6600	1.579E-03	3.627E+00	0.000E+00	0.000E+00	3.632E+00	1.577E-03	1.577E-03	0.000E+00	0.000E+00	0.000E+00	0.000E+00	0.000E+00
0.6800	8.784E-04	3.189E+00	0.000E+00	0.000E+00	3.195E+00	8.761E-04	8.761E-04	0.000E+00	0.000E+00	0.000E+00	0.000E+00	0.000E+00
0.7000	4.736E-04	2.743E+00	0.000E+00	0.000E+00	2.748E+00	4.726E-04	4.726E-04	0.000E+00	0.000E+00	0.000E+00	0.000E+00	0.000E+00
0.7200	2.319E-04	2.318E+00	0.000E+00	0.000E+00	2.317E+00	2.319E-04	2.319E-04	0.000E+00	0.000E+00	0.000E+00	0.000E+00	0.000E+00
0.7400	1.713E-04	1.905E+00	0.000E+00	0.000E+00	1.907E+00	1.713E-04	1.713E-04	0.000E+00	0.000E+00	0.000E+00	0.000E+00	0.000E+00
0.7600	0.000E+00	1.535E+00	0.000E+00	0.000E+00	1.536E+00	0.000E+00						
0.7800	0.000E+00	1.202E+00	0.000E+00	0.000E+00	1.202E+00	0.000E+00						
0.8000	0.000E+00	9.241E-01	0.000E+00	0.000E+00	9.245E-01	0.000E+00						
0.8200	0.000E+00	6.882E-01	0.000E+00	0.000E+00	6.900E-01	0.000E+00						
0.8400	0.000E+00	5.041E-01	0.000E+00	0.000E+00	5.047E-01	0.000E+00						
0.8600	0.000E+00	3.606E-01	0.000E+00	0.000E+00	3.608E-01	0.000E+00						
0.8800	0.000E+00	2.475E-01	0.000E+00	0.000E+00	2.478E-01	0.000E+00						
0.9000	0.000E+00	1.710E-01	0.000E+00	0.000E+00	1.711E-01	0.000E+00						
0.9200	0.000E+00	1.105E-01	0.000E+00	0.000E+00	1.107E-01	0.000E+00						
0.9400	0.000E+00	7.352E-02	0.000E+00	0.000E+00	7.348E-02	0.000E+00						
0.9600	0.000E+00	4.434E-02	0.000E+00	0.000E+00	4.438E-02	0.000E+00						
0.9800	0.000E+00	2.841E-02	0.000E+00	0.000E+00	2.841E-02	0.000E+00						
1.0000	0.000E+00											

OPTICAL EFFICIENCY FOR DISK APERTURE

RADIUS (M)	EFFICIENCY
0.000E+00	0.000E+00
2.000E-02	1.1273E-02
4.000E-02	4.3884E-02
6.000E-02	9.4523E-02
8.000E-02	1.5867E-01
1.000E-01	2.3155E-01
1.200E-01	3.0898E-01
1.400E-01	3.8757E-01
1.600E-01	4.6456E-01
1.800E-01	5.3752E-01
2.000E-01	6.0418E-01
2.200E-01	6.6264E-01
2.400E-01	7.1172E-01
2.600E-01	7.5131E-01
2.800E-01	7.8233E-01
3.000E-01	8.0640E-01
3.200E-01	8.2540E-01
3.400E-01	8.4095E-01
3.600E-01	8.5426E-01
3.800E-01	8.6607E-01
4.000E-01	8.7682E-01
4.200E-01	8.8669E-01
4.400E-01	8.9583E-01
4.600E-01	9.0434E-01
4.800E-01	9.1230E-01
5.000E-01	9.1979E-01
5.200E-01	9.2690E-01
5.400E-01	9.3372E-01
5.600E-01	9.4029E-01
5.800E-01	9.4662E-01
6.000E-01	9.5272E-01
6.200E-01	9.5857E-01
6.400E-01	9.6411E-01
6.600E-01	9.6929E-01
6.800E-01	9.7407E-01
7.000E-01	9.7838E-01
7.200E-01	9.8221E-01
7.400E-01	9.8553E-01
7.600E-01	9.8835E-01
7.800E-01	9.9069E-01
8.000E-01	9.9259E-01
8.200E-01	9.9409E-01
8.400E-01	9.9525E-01
8.600E-01	9.9613E-01
8.800E-01	9.9677E-01
9.000E-01	9.9723E-01
9.200E-01	9.9756E-01
9.400E-01	9.9778E-01
9.600E-01	9.9793E-01
9.800E-01	9.9802E-01
1.000E+00	9.9808E-01

*** INTEGRATION FOR FLAT CIRCULAR TARGET ***

INTEGRATED FLUX USING GAUS8 AND QNC7 = 1.4799E+05 WATTS.

POWER MATRIX (METHOD 1) (INTEGRATIONS OF EACH SET OF 3 X 3 ARRAYS ABOVE)

0.1301E+04	0.1302E+04	0.1302E+04	0.1301E+04	0.1303E+04
0.3381E+04	0.3420E+04	0.3404E+04	0.3388E+04	0.3429E+04
0.4352E+04	0.4523E+04	0.4450E+04	0.4387E+04	0.4573E+04
0.4417E+04	0.4744E+04	0.4576E+04	0.4461E+04	0.4869E+04
0.3967E+04	0.4281E+04	0.4031E+04	0.3930E+04	0.4495E+04
0.3249E+04	0.3234E+04	0.2992E+04	0.3012E+04	0.3461E+04
0.2547E+04	0.1975E+04	0.1847E+04	0.2030E+04	0.2068E+04
0.2068E+04	0.1036E+04	0.1030E+04	0.1307E+04	0.9439E+03
0.1798E+04	0.5838E+03	0.6320E+03	0.8933E+03	0.3731E+03
0.1608E+04	0.4247E+03	0.4698E+03	0.6673E+03	0.1764E+03
0.1431E+04	0.3592E+03	0.3895E+03	0.5241E+03	0.1160E+03
0.1275E+04	0.3180E+03	0.3365E+03	0.4228E+03	0.8937E+02
0.1161E+04	0.2890E+03	0.3004E+03	0.3438E+03	0.7146E+02
0.1097E+04	0.2738E+03	0.2797E+03	0.2781E+03	0.5711E+02
0.1050E+04	0.2627E+03	0.2657E+03	0.2192E+03	0.4454E+02
0.9925E+03	0.2481E+03	0.2495E+03	0.1643E+03	0.3318E+02
0.8924E+03	0.2233E+03	0.2239E+03	0.1134E+03	0.2281E+02
0.7468E+03	0.1870E+03	0.1872E+03	0.7170E+02	0.1438E+02
0.5743E+03	0.1430E+03	0.1437E+03	0.4135E+02	0.8285E+01
0.4020E+03	0.1006E+03	0.1006E+03	0.2130E+02	0.4257E+01
0.2553E+03	0.6386E+02	0.6386E+02	0.9824E+01	0.1965E+01
0.1469E+03	0.3677E+02	0.3677E+02	0.4143E+01	0.8278E+00
0.7628E+02	0.1909E+02	0.1909E+02	0.1569E+01	0.3135E+00
0.3597E+02	0.8993E+01	0.8993E+01	0.5391E+00	0.1077E+00
0.1524E+02	0.3811E+01	0.3811E+01	0.1535E+00	0.3068E-01

TOTAL POWER ON TARGET IS 0.14799E+06 WATTS.

**** SUMMARY RESULTS ****

FACET AREA = 153.8 M**2
 REDUCED BY COS GIVES 148.3 M**2
 FURTHER REDUCED BY SHBL GIVES 148.3 M**2
 POWER INTERCEPTED BY MIRRORS = 0.1483E+06 WATTS.
 NO SHBL EFFECTS INCLUDED.
 SOLAR INSULATION = 0.10000 W/CM**2
 NO. SUNS IN PEAK = 1342.56
 POWER COLLECTED (GAUS8 & QNC7 INTEG) = 0.1480E+06 W
 TARGET OPTICAL EFFICIENCY = 0.9981E+00
 TARGET BLOCKAGE FACTOR = 0.0000E+00
 OPTICAL EFFICIENCY + BLOCKAGE FACTOR = 0.9981E+00

DISTRIBUTION:

Acurex Aerotherm (2)
555 Clyde Avenue
Mountain View, CA 94039

J. Schaefer
D. Duffy

Air Force Rocket Propulsion Lab.
AFRPL/LKCS
Stop 24
Edwards AFB, CA 93523

Jerry Naujokas

Air Research Manufacturing Co.
2525 W. 190 Street
MS T-41
Torrance, CA 90509
Murray Coombs

Australian National University
Department of Engineering Physics
P.O. Box 4
Canberra ACT 2600, AUSTRALIA
Prof. Stephen Kaneff

Barber-Nichols Engineering
6325 West 55th Ave.
Arvada, CO 80002
R. Barber

BDM Corporation
1801 Randolph Street
Albuquerque, NM 87106
W. E. Schwinkendorf

Black & Veatch
P.O. Box 8405
Kansas City, MO 64114
J. C. Grosskreutz

Colorado State University
Ft. Collins, CO 80523
T. G. Lenz

Ford Aerospace
Ford Road
Newport Beach, CA 92663
R. H. Babbe

Georgia Power Co.
7 Solar Circle
Shenandoah, GA 30264
E. Ney

Jet Propulsion Laboratory
4800 Oak Grove Drive
Pasadena, CA 91109
M. Alper

LaCour Kiln Service
P.O. Box 247
Canton, MS 39046
J. A. LaCour

LaJet Energy Co.
P.O. Box 3599
Abilene, TX 79604
Monte McGlaun

McDonnell-Douglas Astronautics
Company (3)
5301 Bolsa Avenue
Huntington Beach, CA 92647
J. B. Blackmon
J. Rogan
D. Steinmeyer

Mechanical Technology, Inc. (2)
968 Albany Shaker Road
Latham, NY 12110
G. R. Dochat
J. Wagner

NASA Lewis Research Center (5)
21000 Brook Park Road
Cleveland, OH 44135
R. Beremand 500-215
R. C. Evans 500-210
R. Hyland 501-17
T. S. Mroz 301-2
R. Shaltens 301-2

New Mexico State University
Physical Science Lab.
Box 3548
Las Cruces, NM 88003
J. McCrary

New Mexico State University
Department of Mechanical Engineering
Las Cruces, NM 88003
G. P. Mulholland

Pacific Northwest Laboratories
P.O. Box 999
Richland, WA 99352
Ray Cavola

Power Kinetics, Inc.
1223 Peoples Avenue
Troy, NY 12180
W. E. Rogers

Rockwell International
Rocketdyne Division
6633 Canoga Ave.
Canoga Park, Ca 91304
Lou Pidcoke

Rockwell International
Space Station Systems Division
12214 Lakewood Blvd.
Downey, CA 90241
I. M. Chen

Sanders Associates
MER 15-2350
C.S. 2035
Nashua, NH 03061-2035
Jim Kesseli

Science Applications
International Corp.
10401 Roselle Street
San Diego, CA 92121
Barry Butler

Solar Energy Research Inst. (4)
1617 Cole Blvd.
Golden, CO 80401
B. P. Gupta
J. Thornton
D. Johnson
M. Murphy

Solar Kinetics, Inc.
P.O. Box 47045
Dallas, TX 75247
J. A. Hutchison

Solar Steam
Suite 400
Old City Hall
625 Commerce Street
Tacoma, WA 98402
D. E. Wood

Stirling Thermal Motors
2841 Boardwalk
Ann Arbor, MI 48104
B. Ziph

Sundstrand ATG (2)
P.O. Box 7002
Rockford, IL 61125
Bob Lauson
Larry McGee

Texas Tech University
Dept. of Electrical Engineering
P.O. Box 4439
Lubbock, TX 79409
E. A. O'Hair

University of Houston
Energy Laboratory; SPA
Houston, TX 77004
Lorin Vant-Hull

University of Minnesota
Mechanical Engineering Dept.
111 Church St. SE
Minneapolis, MN 55455
E. A. Fletcher

University of New Mexico (2)
Department of Mechanical Engr.
Albuquerque, NM 87131
M. W. Wilden
W. A. Gross

U.S. Department of Energy (4)
Albuquerque Operations Office
P.O. Box 5400
Albuquerque, NM 87185
D. Graves
R. Y. Lowrey
J. Weisiger
N. Lackey

U.S. Department of Energy
Office of Solar Heat Technologies
Forrestal Building
Washington, DC 20585
Fred Morse

U.S. Department of Energy
Office of Solar Heat Technologies
Forrestal Building
Washington, DC 20585
C. Carwile

U.S. Department of Energy
Division of Solar Thermal Tech.
Forrestal Building
Washington, DC 20585
Howard S. Coleman
R. Shivers
S. Gronich
C. Mangold
M. Scheve
F. Wilkins

Veda Inc.
1317 Del Norte Road
Camarillo, CA 93010
C. Carrera
T. Reed

1000 W. F. Brinkman
1500 W. Herrmann
1510 J. W. Nunziato
1511 G. G. Weigand
1512 J. C. Cummings
1512 R. D. Skocypec
1513 B. D. Boughton (5)
1513 R. G. Gross
1513 R. E. Hogan
1513 D. W. Larson
1513 A. C. Ratzel (10)
1520 W. Herrmann, Acting
1530 L. W. Davison
1540 W. C. Luth
1550 R. C. Maydew
2540 G. N. Beeler
2541 J. P. Abbin
2541 C. E. Andraka
3141 S. A. Landenberger (5)
3151 W. L. Garner (3)
3154 C. H. Dalin (28) for DOE/TIC
3160 J. E. Mitchell
6200 V. L. Dugan
6220 D. G. Schueler
6221 E. C. Boes
6222 J. V. Otts
6223 G. J. Jones
6224 D. E. Arvizu
6225 H. M. Dodd
6226 J. T. Holmes
6227 J. A. Leonard (20)
6227 B. Baker (2)
6227 R. B. Diver (4)
6227 T. R. Mancini (4)
8024 P. W. Dean